Origin of the nonideal structure in Ka-band spectra since 2007

NRAO GBT Memo 266

December 22, 2009

A.I. Harris[a] and A.J. Baker[b]

[a]University of Maryland, [b]Rutgers University

Abstract

We show that the baseline ripple and excess noise in Zpectrometer spectra are caused by residual reflection-related imbalances within the Ka-band receiver's waveguide components and optics. The imbalances also affect Spectrometer spectra. We find that optical coupling to the telescope plays some role, but that temperature drifts in the external electronics, input matching of the LNAs, cryostat modes, and coupling between the horns are not important for our standard beam switching time of 10 seconds. The origin we suggest explains the observed fast drifts on the telescope, and slow and no drifts in the lab, but does not explain the occasional glitches apparent in long lab measurements.

1 Introduction

Since its first real commissioning in Fall 2007, after the Ka-band receiver's front end was rebuilt for greater symmetry, Zpectrometer spectra have shown occasional ripple and have always had excess noise. The ripple is coherent across all three Zpectrometer sub-bands (Fig. 1), which pointed to an origin in the receiver or early in the Zpectrometer's IF system. The ripple has an approximate period of 300 MHz across the spectrum, but is not exactly constant in either frequency or wavelength space. Amplitude modulation across the spectrum and phase shifts with time suggest an origin in a small band of frequencies. Averaged over a typical 4 minute integration, its amplitude has ranged from nearly undetectable to severe (Fig. 1 shows a series of severe but not atypical cases). While filtering in the Fourier domain is possible to treat the symptoms, it further corrupts the spectrum, is not possible for continuum calibration sources, and reduces the signal to noise ratio. The ripple's presence indicates an underlying problem that we should understand. It is also possible that the ripple shares a common root cause with another problem: the noise in spectra is 2 to 3 times higher than expected from the radiometer equation (Fig. 2; dashed lines show noise levels scaled from the radiometer equation) [1]. While Zpectrometer observations have been very successful for lines brighter than about 1 mJy, and are possible for lines of a few hundred μJy, the observing efficiency with excess noise and ripple have made observations of weak lines impractical.

In the following, we use data from Galen Watt's exploratory lab test program (July through November 2009) and data from astronomical observations with the Zpectrometer in the Fall/Winter seasons of 2007 through 2009. Dates for lab data correspond to those in the test series database[1]. The measurements concentrated on sub-band zp1, the "master" correlator with frequency range in a good part of the receiver's band. The analysis examines the time series data from the correlator lags, either directly, by lag-lag covariances, or through their Allan variances [2, 3].

[1]On the Green Bank computer system under /users/gwatts/DataAnalysis/Zpectrometer

2 Results

2.1 Receiver input imbalance

The strongest evidence for a connection between instability and front end imbalance is that lags with high fluctuations, measured by the Allan variance, have systematically larger deviations from the ideal of zero in the cross-correlation functions (CCFs). This is clearest in observations on the sky, where the total power can fluctuate over relatively short timescales. Figure 3 is a plot of the Allan variance vs. lag number at 20 seconds lag; this is a kind of power spectrum that shows power fluctuation on a timescale of interest for the Zpectrometer's usual 10 second beamswitch period. The zero (total power) lag falls at lag 250 to 251. A power-law decrease in variance from the zero lag to about lag 200 is reminiscent of $1/f$ noise. Vertical dashed lines indicate peaks selected in the spectrum. Figure 4 is the corresponding plot of the CCF amplitude vs. lag number with the same lags marked. The correlation between the two is even clearer in a plot of Allan variance vs. CCF squared, Figure 5, with the numbers marking the position of each lag in the scatter plot and the blue numerals indicating those lags marked with lines in Figures 3 and 4. While most of the lags are clustered near zero variance and amplitude, Figure 5 shows a clear correspondence in Allan variance and CCF amplitude in a tail of high-amplitude lags that includes all of the lags with peaks.

Figures 6 through 8 summarize the same analysis for data from the telescope, showing the same correspondence, but with different lags affected. Figures 9 through 11 examine the time series for lag 221, a lag that not only has a high fluctuation amplitude, but a lag that corresponds to a 300 MHz period (lags 220 and 222 correspond to frequencies near 300 MHz and are also high in amplitude, see Fig. 6). Figure 9 shows an irregular fluctuation pattern in time. Figure 10 color-codes the 240 second integrations on the source and reference positions with blue and red, respectively: telescope motion has no discernible effect on the fluctuations. Figure 11 shows a section of the data with an expanded time scale: there is structure at timescales from a few to many tens of seconds. Figures 12 through 20 give the time sequences for a range of lags for comparison, all on the same scales.

While the fluctuations in observations on the sky are often erratic, in two of the six cases we have examined there is strong periodic structure. Figure 21 shows the clearest example, a sawtooth waveform with a well-defined 344 second period that emerges from somewhat irregular fluctuations. (The other example has a similar basic waveform and a 343 second period, essentially identical timing.) The vertical lines in Figure 21 mark pointing cycles, gaps of about five minutes with relatively large elevation changes. Although the phase of the sawtooth seems to be continuous through the pointings, close examination shows extra structure at the pointing near 6700 seconds, so the apparent continuity is probably coincidence. A 344 second period matches neither the integration time of 240 seconds nor the elapsed time per integration of about 514 seconds for a source-reference cycle. The structure could be related to an air conditioning cycle, although we measured little to no sensitivity to temperature changes in lab tests (Sec. 2.2), to antenna surface adjustments or secondary motion, or to something else. The sawtooth appears in only the few most unstable lags, and does not appear in the zero lag. G. Watts discovered that the IF plate temperature oscillated by about 6° C, but any effect there would likely affect more lags, including the zero lag, and again should be present in warm electronics temperature tests.

2.2 *Temperature effects, warm electronics*

A series of measurements on 27 August 2009 showed that the warm bias and high frequency electronics are insensitive to temperature changes. We first fanned ambient air across different parts of the receiver, then blew compressed air through the card cages and on amplifiers, multipliers, and other high-frequency components. There was no obvious correlation with any of the actions and changes in the time-sequence lag data. These measurements confirmed the lack of sensitivity G. Watts measured with hot air when the instrument was on the telescope.

2.3 *Optical coupling*

Figure 22 is a series of normalized CCFs showing optical coupling effects on the receiver in the first set of lab measurements[2]. The blue curve is the baseline: the receiver in the lab but still under vacuum after being removed from the telescope. The magenta curve shows the CCF with the cryostat at atmospheric pressure but everything otherwise the same; the changes in the CCF are minor. The CCF changed dramatically when the Zotefoam vacuum window was removed, especially at lag 223 and 209, with more minor changes at the lags between. Lags above lag 225 were largely unaffected. This measurement shows that standing waves between the front-end components and the window are important for structure from approximately lags 205 to 225.

The receiver is sensitive to the impedance that the telescope itself presents. Figure 23 contains plots of the normalized CCFs in the lab under vacuum (blue, as before) and on the telescope[3]. The CCF on the telescope was stable over the two seasons observing covered in this memo, and the plot is a good representative of the CCFs. The changes in CCF are all real, if mostly minor, except for the large changes near lag 210 and lags 220 to 226 (the change at lag 251 is in the zero lag and is due to the temperature difference between the horns). Such large changes between the telescope and lab implies either that optical coupling to the telescope plays a role or that there were reflections from the Eccosorb load in the lab that was specific to the test setup.

2.4 *Cryostat cavity modes*

One proposal to explain the spectral structure in both Zpectrometer and Spectrometer data is that changes in the cryostat dimensions, caused by mechanical stress or thermal expansion, changes the standing wave structure in the cryostat [4]. Microwave absorber lines the interior of the cryostat's radiation shield for this reason.

Cryostat heating does leave a signature in lag stability. Figure 24 shows the effect of controlled heating[4]: a heating tape wrapped around the cryostat delivered several hundred watts to the cryostat can for several minutes at a time. The brown curve is the baseline, an Allan variance spectrum measured before heating. Two sets of heat pulses followed, each with duration of a few minutes (blue and then green curves). There is little change at lag numbers above 200, with the largest change a fairly uniform variance increase for lag numbers below about 180. The characteristic of the effect is most visible at long lag times (here 295 seconds): a strong dip centered at about lag 200. Figure 25 shows the same data for a 20 second lag time, appropriate for our observations. Very little change is present, and all at low lag numbers. Such

[2] 1 July 2009
[3] 8C73_18, dharma, 12 Dec. 2008
[4] 12 Nov. 2009

changes would add some high-frequency noise across the spectra but have very little influence on the ripple. These measurements confirm less controlled measurements from heat gun heating[5].

The CCFs are sensitive to the presence of the 50 K shield[6], especially in the low and mid lags. Interestingly, the sensitivity was present even when the loads stuffed with absorber, indicating coupling through paths other than the horns.

We believe that these measurements rule out cryostat modes as the root of the problem. First, the effect is on the wrong lags; second, the effect is small over important timescales even with step function heating of several hundred watts, far from the thermal environment on the telescope; third, we saw no large change in the ripple or noise whether the cryostat was insulated or not on the telescope; fourth, the CCF changes little with the stress relief from bringing the cryostat back to atmospheric pressure[7]; and fifth, there is no large change in stability whether the cryostat cavity is present or not.

2.5 Amplifier input impedance

Measurements with and without isolators in front of the amplifiers[8] show no major changes in stability. Adding isolators after the horns creates considerable structure in lags 225-226 (Fig. 26). This probably points to standing waves between the horns and the hybrid (see also Sec. 2.3). A resonance seems to appear when the isolators are between the horns and hybrid, perhaps because the isolators are not identical and do not cancel reflections as well as the geometrical cancellation provided by the swept bends alone.

2.6 Horn proximity effects

G. Watts noted that the horn apertures are within a few millimeters of metal structure in the radiation shields and investigated the possibility that the horns and cryostat structure interacted[9]. His investigation, which included adding absorber to the shields near the aperture and additional screens between the horns, indicated that this kind of coupling is not a large effect. He does suggest that fringing fields could bear on the observation that the beams, measured with the DCR pointing system, are somewhat elliptical.

We agree with his analysis. As noted in the section on cryostat modes, stability times do not depend strongly on whether the cryostat and therefore shields near the apertures are in place or absent.

2.7 Radome and horn motion

We established that radome motion changes the standing wave pattern by physically pushing the radome and pressurizing it during lab tests[10]. We have also been concerned that the mechanical constraints inside the cryostat might allow the horns to move slightly with telescope elevation to change the standing wave structure. Both of these motions could provide additional structure during observations on the telescope, but they are not the prime problem the lab tests investigate: there is no wind in the lab and the receiver does not tilt.

[5] 8 Oct. 2009
[6] 9 Oct. 2009
[7] Figure 22
[8] 10 Aug. 2009, 14 Aug. 2009
[9] Dates around 19 Oct. 2009
[10] 27 Aug. 2009

While it is worth considering remediation, the magnitude of the wind and tilt problems is not really known. Changes, such as replacing the vacuum window and fabric radome with a rigid Teflon structure, may cause more problems than they solve. If the Teflon-air interfaces do not match the microwaves' radii of curvature then the window will act as a weak lens, changing the focus, beam separation on the sky, and perhaps the illumination of the telescope. If the radii are even close to matching the phase fronts, then the window will produce strong standing waves.

3 Discussion

While many things will affect the spectra at some level, we are looking for the dominant problems. Figures 5 and 8 are compelling evidence that the dominant problem is receiver imbalance, which causes both excess noise and ripple. The figures show an underlying structure, similar to a $1/f$ noise spectrum, which appears in spectra as fluctuating baseline structure. Discrete spikes in the lags from 220 to 222 cause the 300 MHz ripple. Other ripple components are present but are an order of magnitude smaller than the main ripple. Many other mechanisms are doubtless present but, following the analysis above, do not contribute strongly in the Zpectrometer's usual observing mode.

This conclusion is not surprising. Comparison of performance in Figures 4 (CCF) and 3 (spectra) of our report on the original investigation into Ka-band receiver problems [5][11], confirmed by by measurement [6], showed the importance of balance for the receiver. The 2007 rebuild reduced the receiver's input waveguide circuit's imbalance, bringing the spectroscopic performance from unusable to usable, but some imbalance was and is still present.

As before, we suggest that reflection losses from impedance mismatches are responsible for the imbalance. Reflection losses between components can be sensitive to small changes in physical dimensions both inside the waveguide structure and outside, especially if multiple reflections are involved. The strong ripple is likely to be the result of a resonance involving the receiver coupling to the telescope optics. Figures 7 and 6, taken together, show the characteristic of a resonance: a rapid change from a strong negative to positive signal in the CCF as the phase wraps through the resonance. A relatively high-Q resonance will produce high variance if the center frequency shifts in time.

Although we are not aware of any measurements of the reflection coefficients of individual receiver components, we can get a sense of the input hybrid's contribution to imbalance from published specifications [7]. Millitech quotes a maximum VSWR for its CMT-28 as 1.5 or 1.6:1 depending on the input port, corresponding to a voltage reflection coefficient of 0.20–0.23, or a return loss of 14.0–12.7 dB. (This specification seems to apply to both 60% and 90% bandwidth versions, which is a little puzzling.) In any case, the maximum reflection is large. It would be possible to improve the match substantially by changing to a 90° hybrid. Srikanth and Kerr [8], designed, fabricated, and measured properties of a 6-branch 90° hybrid in the WR-10 band and give scaling recipes. From their Figure 1, the measured input return loss is -24 dB across the band, corresponding to a 0.06 reflection coefficient (VSWR 1.13:1). The hybrid has flat and excellent phase balance ($< 1°$ across most of the band, $< 2°$ over the entire band), and a smoothly varying amplitude balance < 1 dB p-p across almost whole band. A 90° hybrid has the additional advantage of eliminating some noise terms in a correlation receiver configuration [9]. Adding a pair of 90° hybrids, connected to provide an additonal 90° differential phase shift after the Zpectrometer tap but before the second hybrid, would make electronic beamswitching

[11] Data in this memo correspond to slot 2 in [5]

possible for the CCB and Spectrometer.

Imbalance explains the system behavior in the lab and on the telescope. On the sky, the input temperature changes quickly and irregularly, or, apparently, regularly due to an unknown effect. In the lab, the input temperatures drift slowly. Lab measurements of thermalized waveguide loads in place of the horns were extremely stable. Even with terminations, though, there is an example of drifts when one load had thermalized and the other not[12], ruling out simple impedance mismatches as an origin.

Imbalance does not explain the occasional glitches seen in the lab CCFs, but those are rare. Some correlator sub-bands have occasional (about one part in 10^5) bad readouts of a few lags as well, probably due to a connector problem. Logic in the reduction software catches these and any other large glitches.

4 Conclusion

Without reducing the nonideal noise and ripple there is little point in hoping for sensitive Ka-band spectra. Although Zpectrometer noise integrates down for many hours, the excess noise makes observations too inefficient for lines weaker than about 1 mJy. Even without corresponding data on Spectrometer performance, we do not expect a major difference in performance between the total power (Spectrometer) and correlation (Zpectrometer) modes. Comparison of gain terms in equations (3) and (A.1) in [10] show that imbalance affects spectra from both back ends.

If further effort is invested in this project, we would suggest network analyzer measurements of all waveguide components, then modeling the circuit to identify the parts that interact to produce the largest standing waves. A less thorough approach would be to identify the components with the largest reflections and to replace them with better components. Replacing the input magic-tee hybrid with a broadband 90° hybrid would be a first step in this direction.

Acknowledgments

This work was supported in part by the National Science Foundation grant AST-0503946 to the University of Maryland and by the University of Maryland.

[12] 14 Jul 09, t4

References

[1] A. Harris and A. Baker, "Zpectrometer observing technical notes." Report, 2009. http://www.astro.umd.edu/∼harris/kaband/zp_info_0905.pdf.

[2] D. W. Allan, "Statistics of atomic frequency standards," *Proc. IEEE*, vol. 54, pp. 221–230, 1966.

[3] R. Schieder and C. Kramer, "Optimization of heterodyne observations using Allan variance measurements," *Astron. Astrophys.*, vol. 373, pp. 746–756, 2001.

[4] R. Norrod, "Cryostat cavity noise and the impact on spectral baselines." NRAO Electronics Division Internal Report No. 318, 2007.

[5] A. Harris, S. Zonak, and G. Watts, "Symmetry in the Ka-band correlation receiver's input circuit and spectral baseline structure." NRAO Green Bank Telescope memo series No. 248, 2007. https://safe.nrao.edu/wiki/bin/view/GB/Knowledge/GBTMemos.

[6] A. Harris, S. Zonak, and G. Watts, "Brief summary of results from modified Ka-band receiver tests." Report, 2007. http://www.astro.umd.edu/∼harris/kaband/aug07_report.txt.

[7] Millitech Inc., "Series CMT magic tee hybrid couplers." Data sheet, 2004. http://www.millitech.com/pdfs/specsheets/IS000058-CMT.pdf.

[8] S. Srikanth and A. Kerr, "Waveguide quadrature hybrids for ALMA receivers." ALMA Memo 343, 2001. http://www.alma.nrao.edu/memos/index.html.

[9] A. Harris, "Spectroscopy with multichannel correlation radiometers," *Rev. Sci. Inst.*, vol. 76, pp. 4503–+, May 2005.

[10] A. Harris, S. Zonak, G. Watts, and R. Norrod, "Design considerations for correlation radiometers." NRAO Green Bank Telescope memo series No. 254, 2007. https://safe.nrao.edu/wiki/bin/view/GB/Knowledge/GBTMemos.

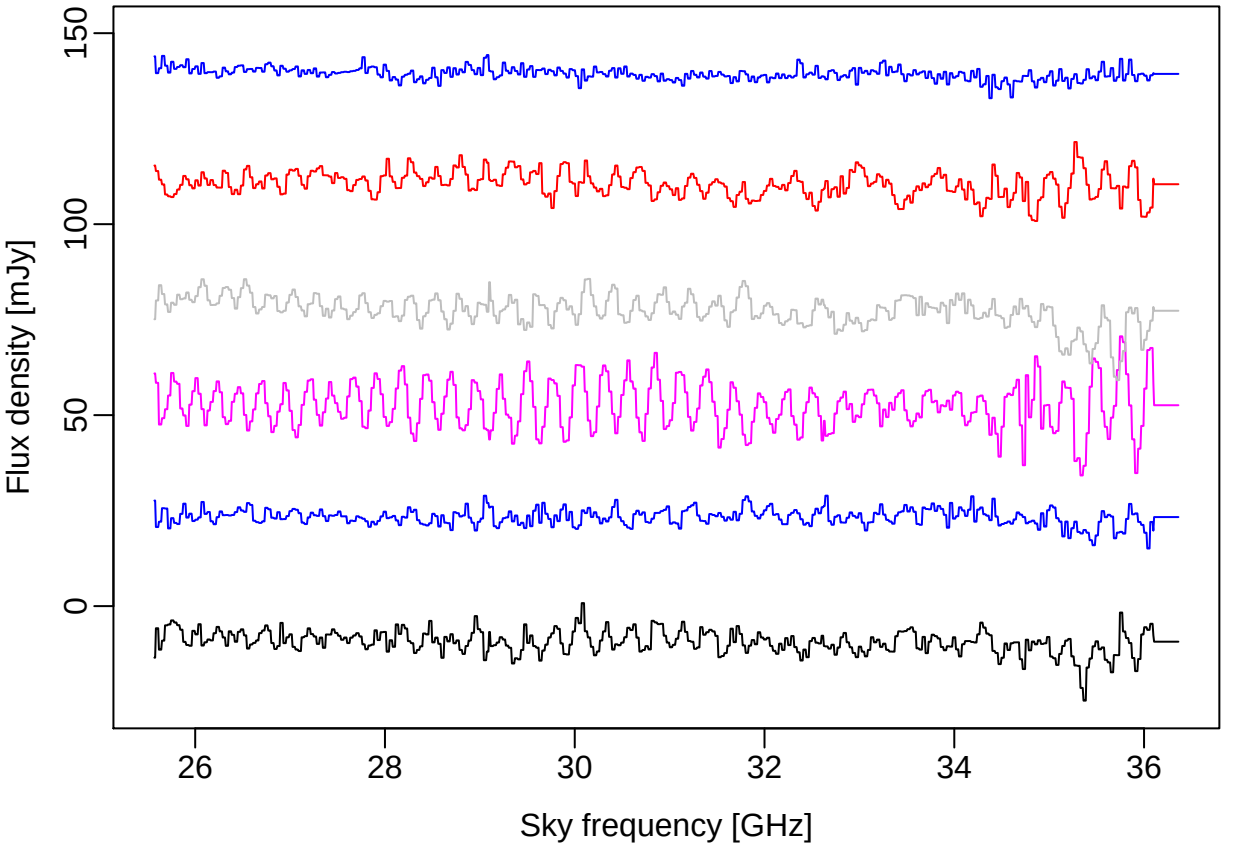
Flux density [mJy]
150
100
50
0
26
28
30
32
34
36
Sky frequency [GHz]

Figure 1

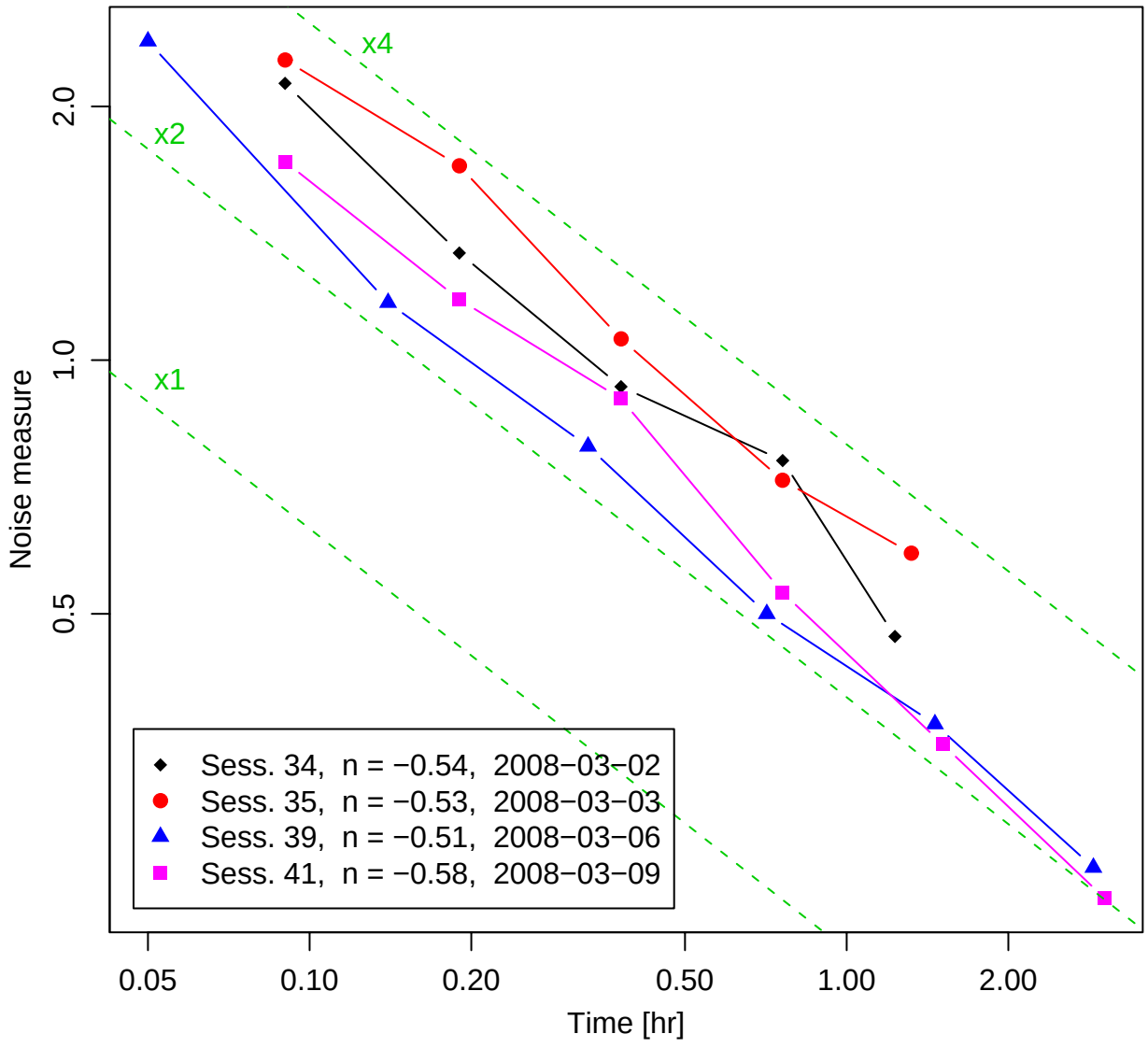
x4
x2
x1
Noise measure
2.0
1.0
0.5
0.05
0.10
0.20
0.50
1.00
2.00
Time [hr]
Sess. 34, n = −0.54, 2008−03−02
Sess. 35, n = −0.53, 2008−03−03
Sess. 39, n = −0.51, 2008−03−06
Sess. 41, n = −0.58, 2008−03−09

Figure 2

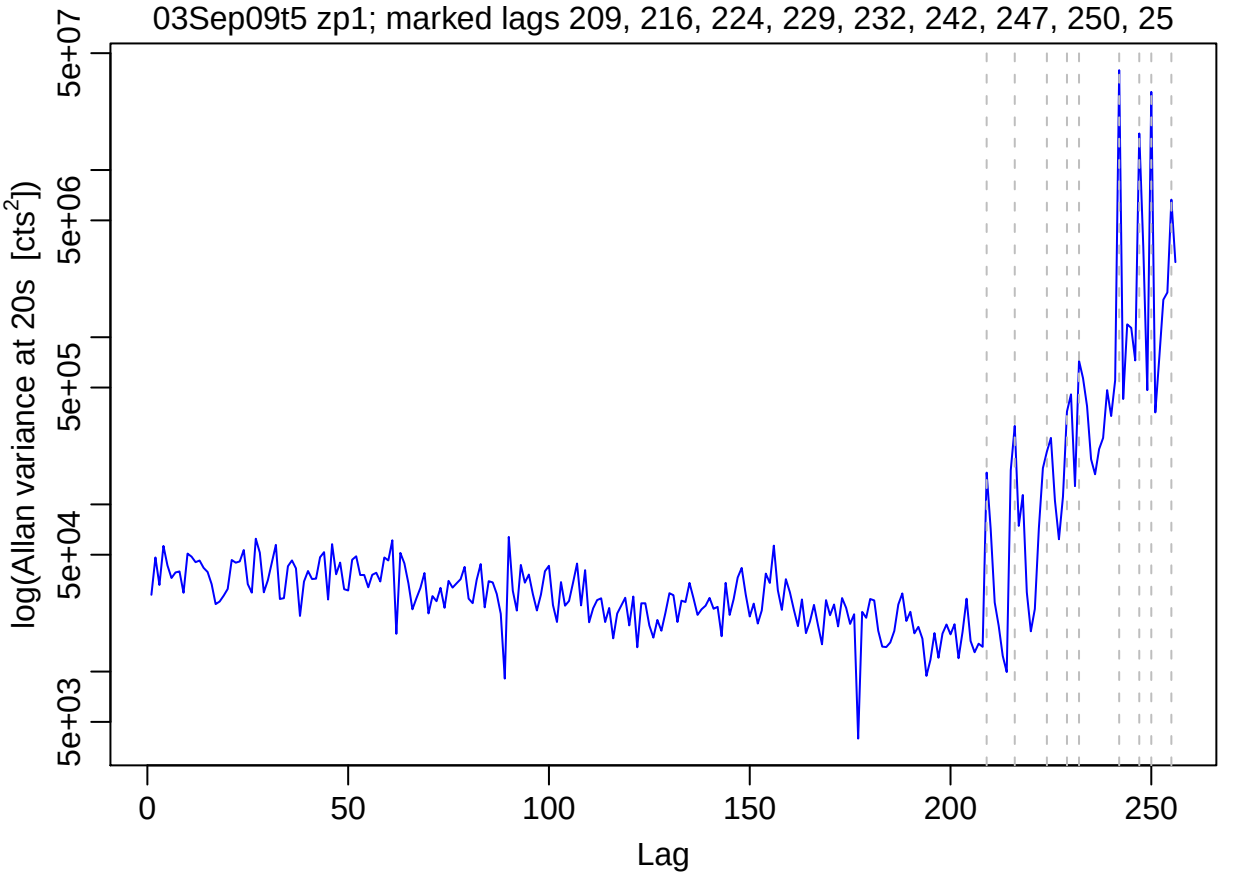
03Sep09t5 zp1; marked lags 209, 216, 224, 229, 232, 242, 247, 250, 25
log(Allan variance at 20s [cts^2])
5e+03
5e+04
5e+05
5e+06
5e+07
0
50
100
150
200
250
Lag

Figure 3

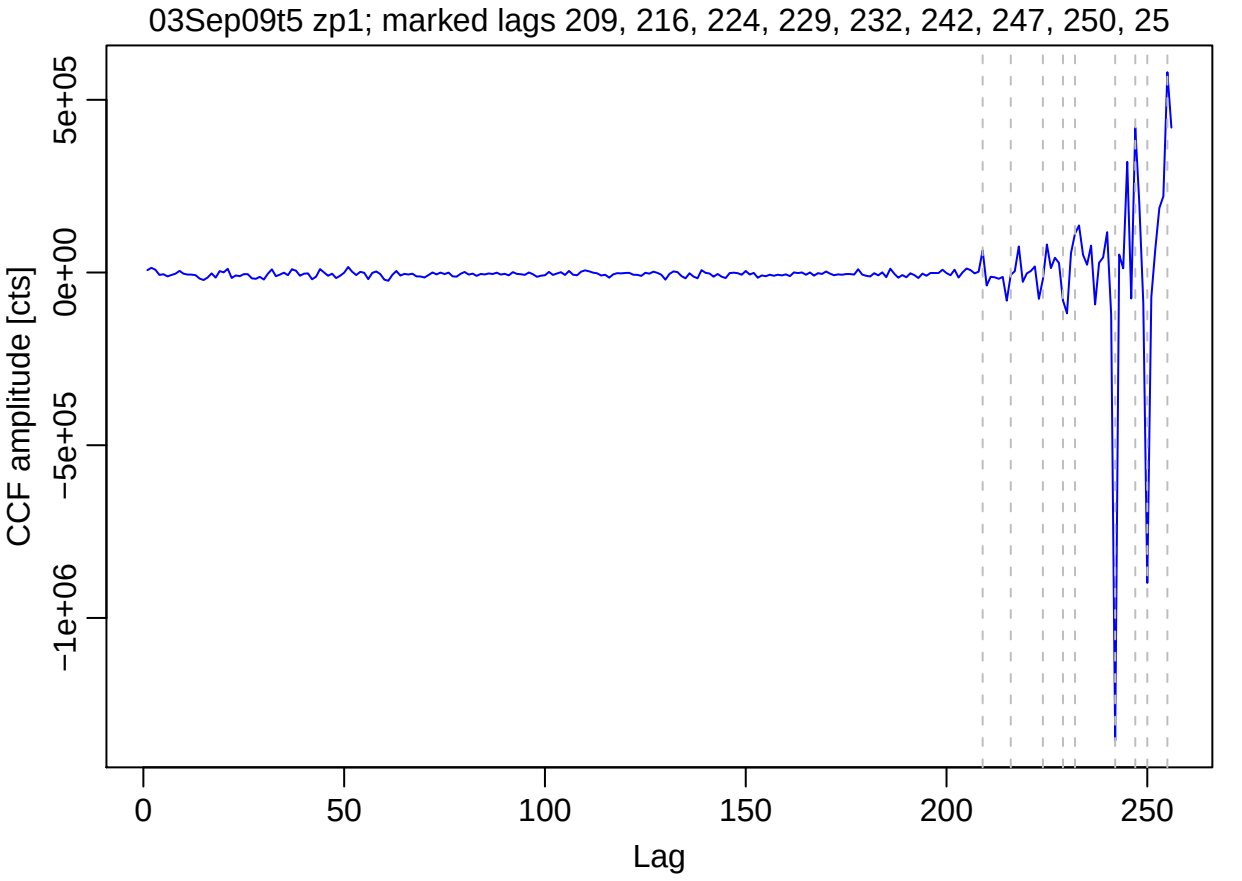
03Sep09t5 zp1; marked lags 209, 216, 224, 229, 232, 242, 247, 250, 25
CCF amplitude [cts]
5e+05
0e+00
−5e+05
−1e+06
0
50
100
150
200
250
Lag

Figure 4

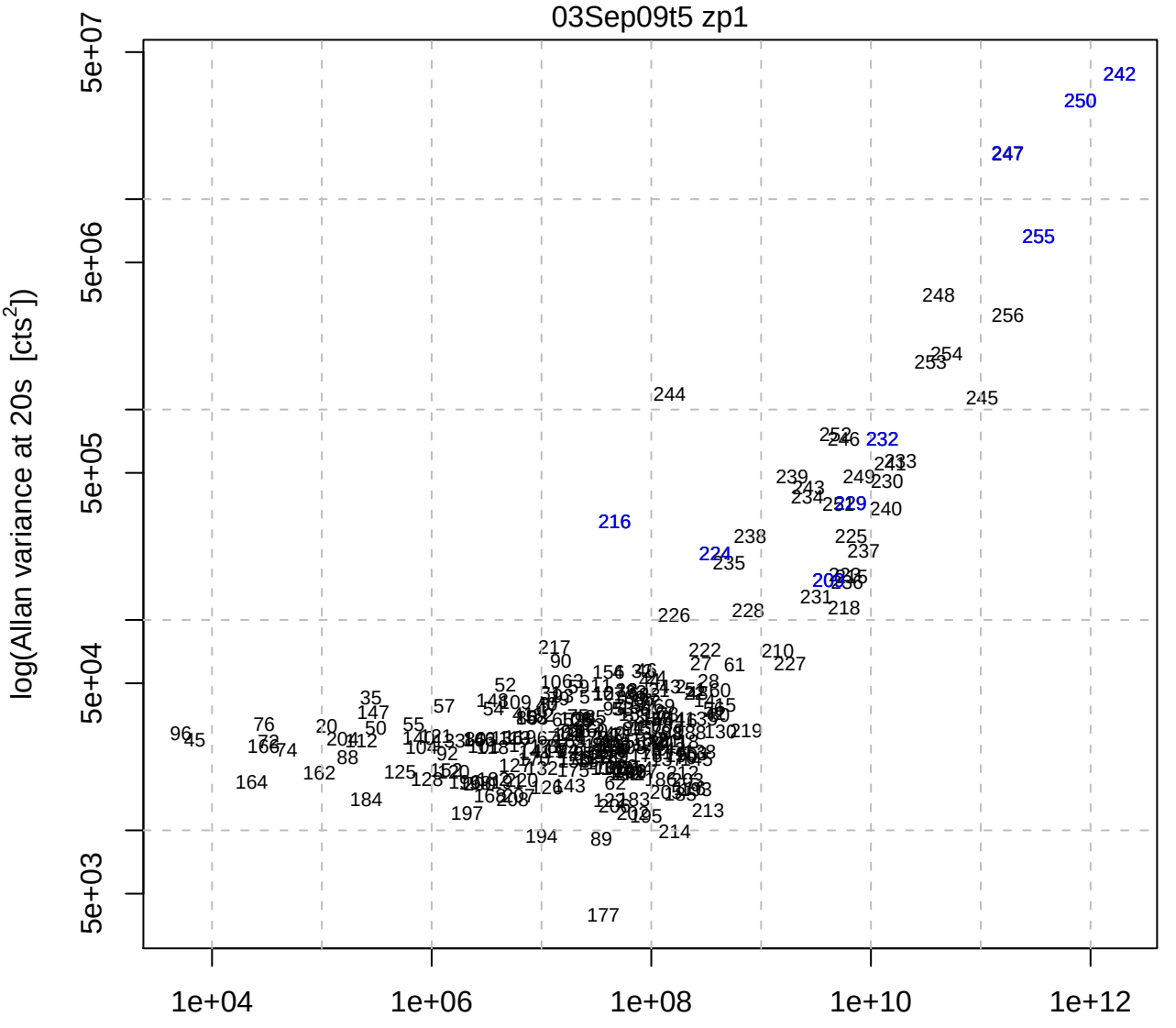
03Sep09t5 zp1
log(Allan variance at 20s [cts^2])
5e+07
5e+06
5e+05
5e+04
5e+03
1e+04
1e+06
1e+08
1e+10
1e+12
log(CCF^2 [cts^2])

Figure 5

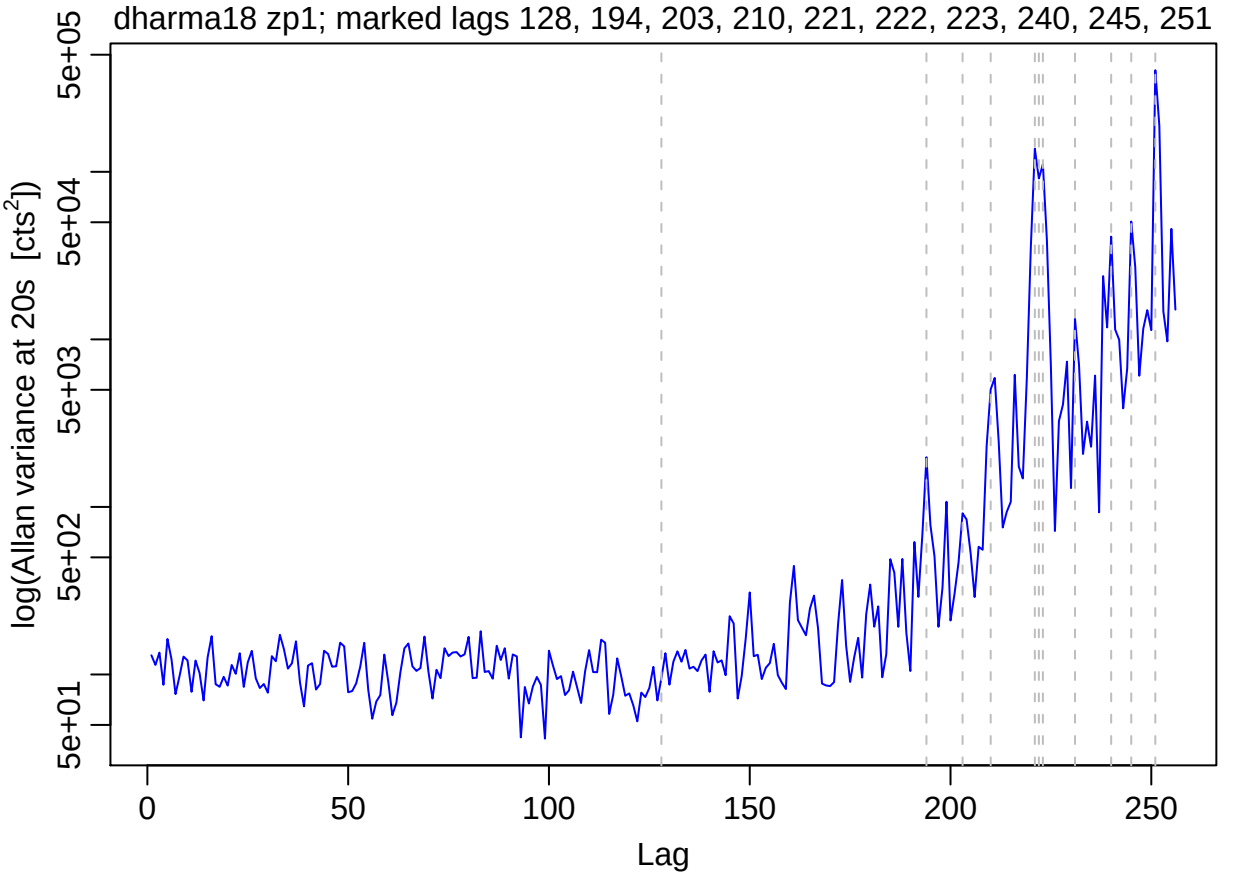
dharma18 zp1; marked lags 128, 194, 203, 210, 221, 222, 223, 240, 245, 251
log(Allan variance at 20s [cts^2])
5e+01
5e+02
5e+03
5e+04
5e+05
0
50
100
150
200
250
Lag

Figure 6

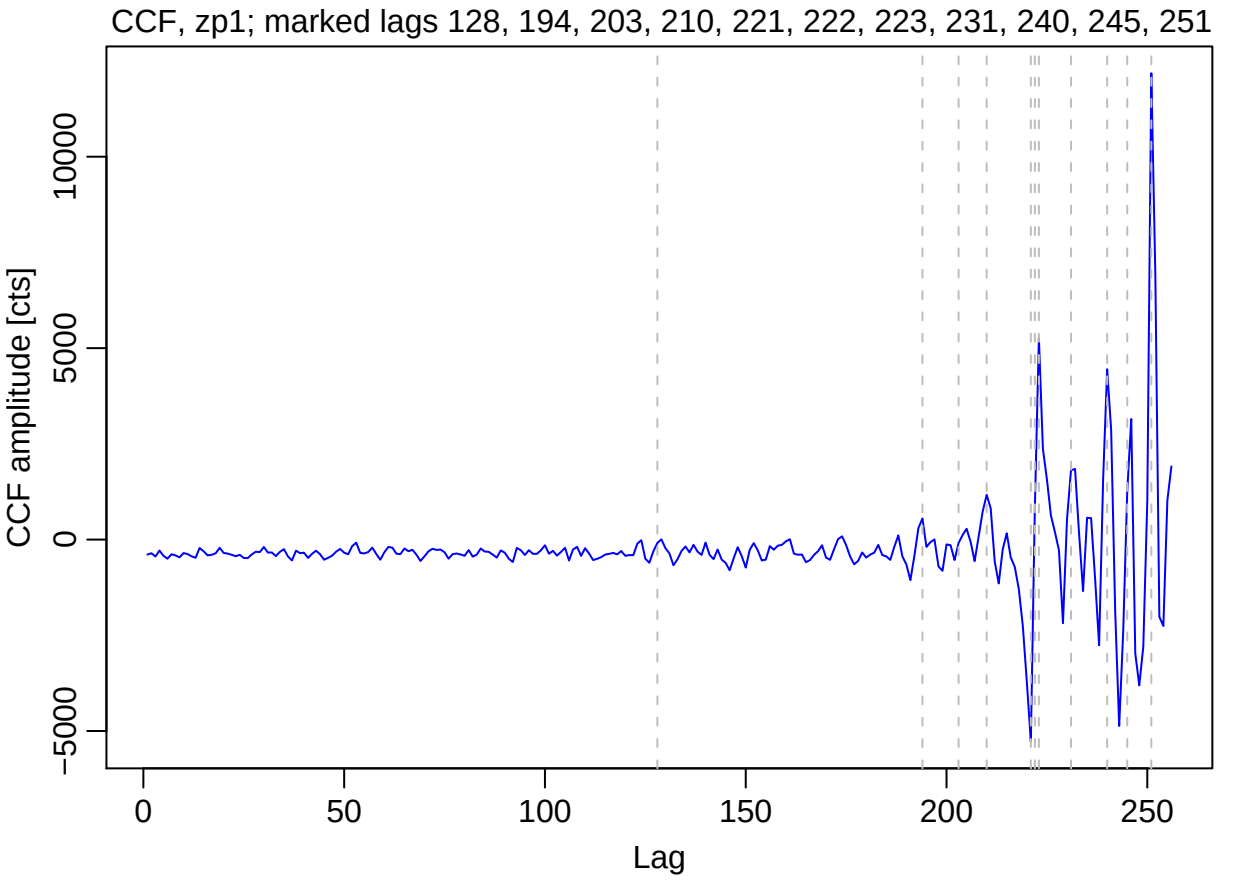
CCF, zp1; marked lags 128, 194, 203, 210, 221, 222, 223, 231, 240, 245, 251
CCF amplitude [cts]
10000
5000
0
−5000
0
50
100
150
200
250
Lag

Figure 7

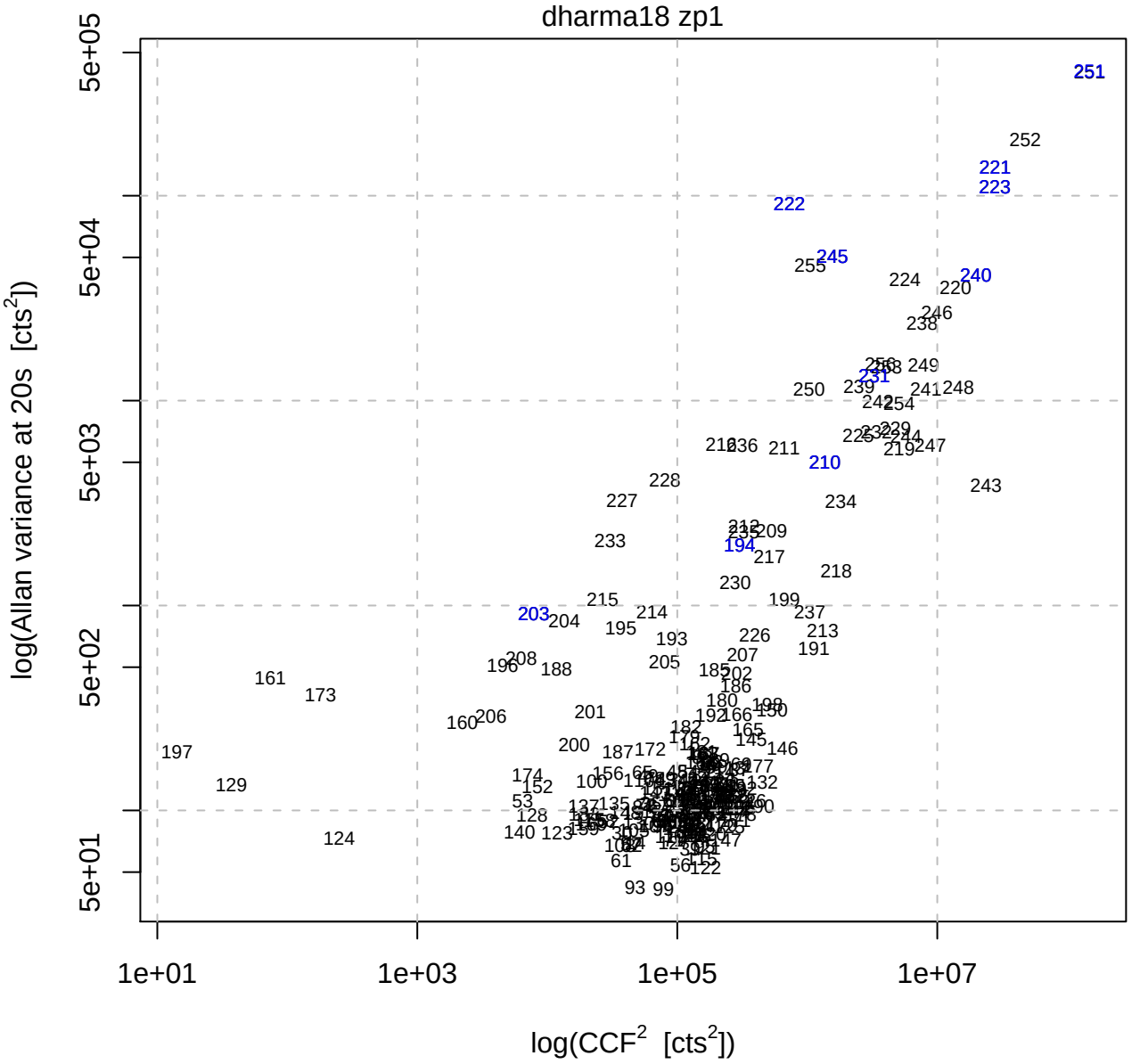
dharma18 zp1
log(Allan variance at 20s [cts^2])
log(CCF^2 [cts^2])
5e+05
5e+04
5e+03
5e+02
5e+01
1e+01
1e+03
1e+05
1e+07

Figure 8

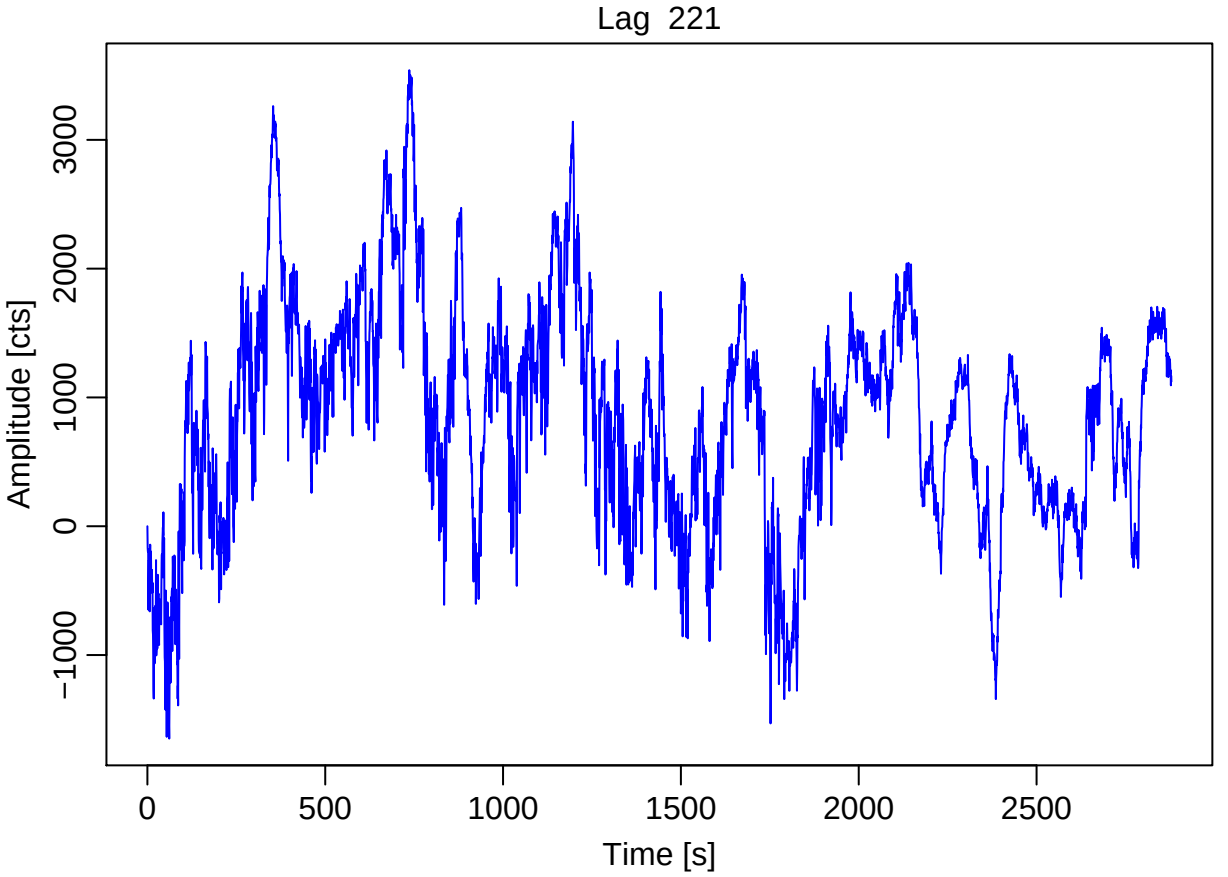
Lag 221
Amplitude [cts]
3000
2000
1000
0
−1000
0
500
1000
1500
2000
2500
Time [s]

Figure 9

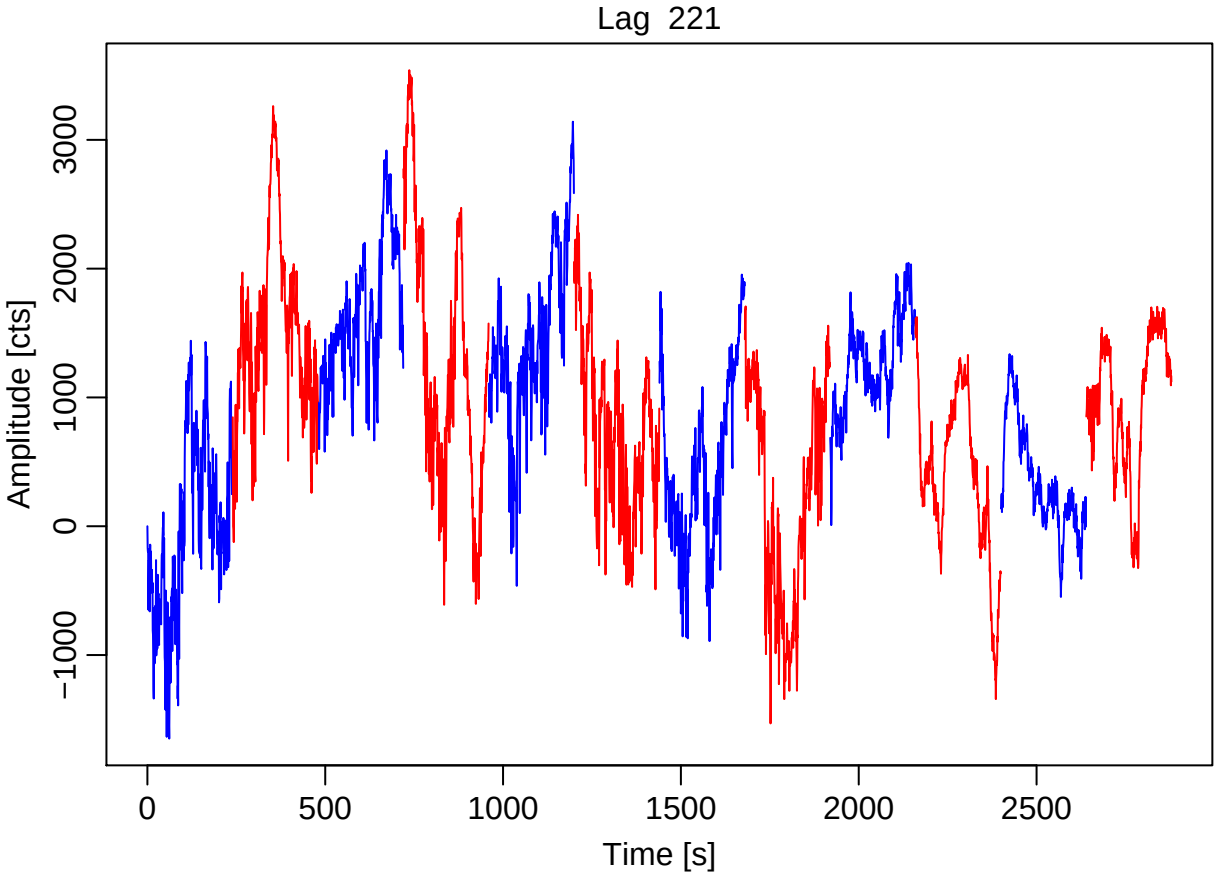
Lag 221
Amplitude [cts]
−1000
0
1000
2000
3000
0
500
1000
1500
2000
2500
Time [s]

Figure 10

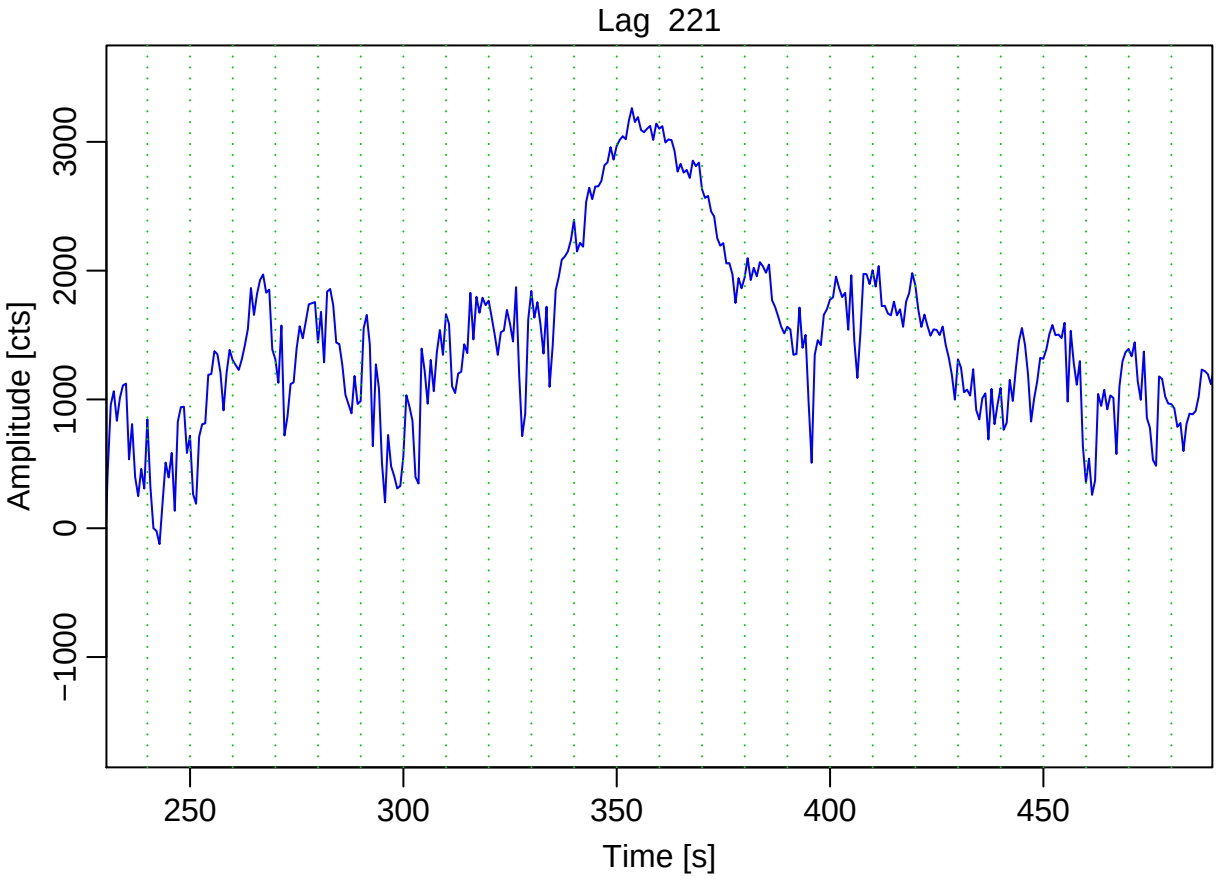
Lag 221
Amplitude [cts]
3000
2000
1000
0
−1000
250
300
350
400
450
Time [s]

Figure 11

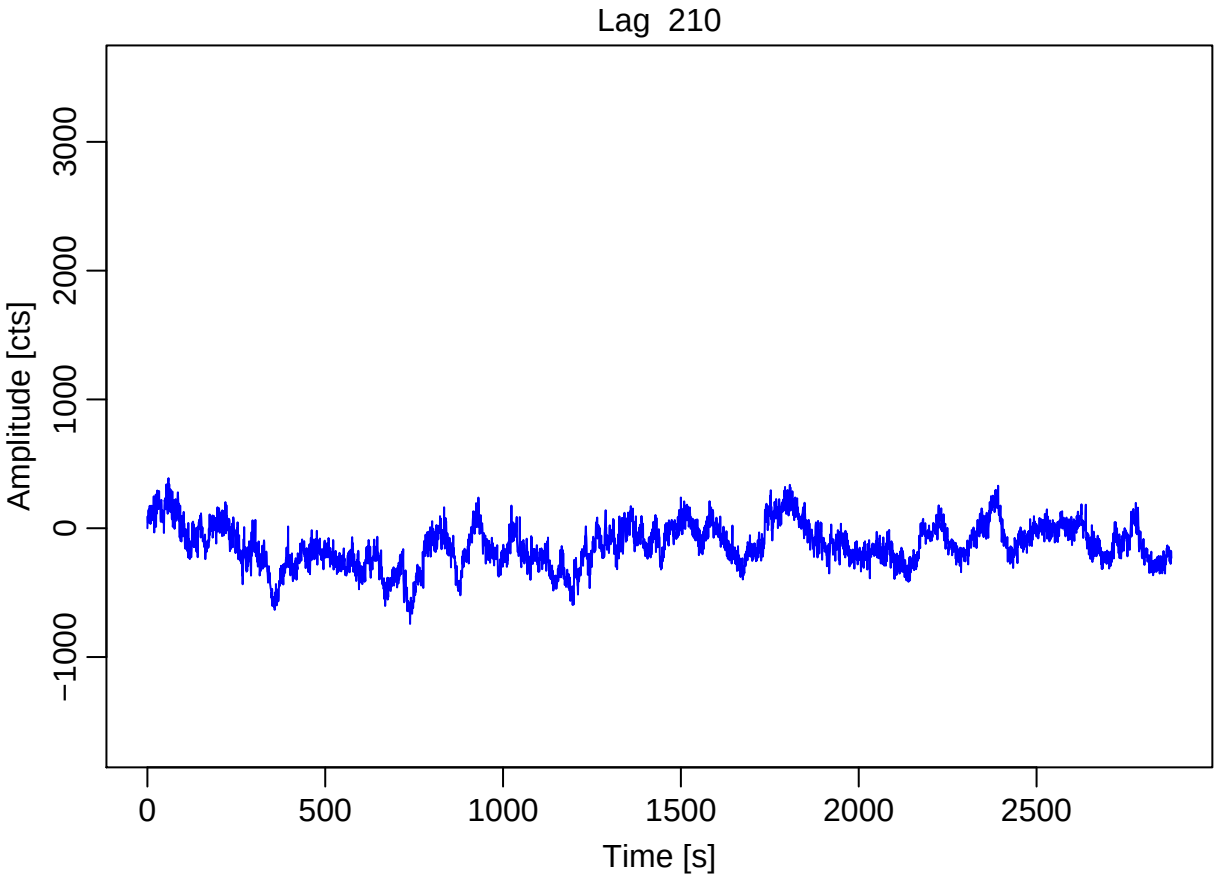
Lag 210
Amplitude [cts]
3000
2000
1000
0
−1000
0
500
1000
1500
2000
2500
Time [s]

Figure 12

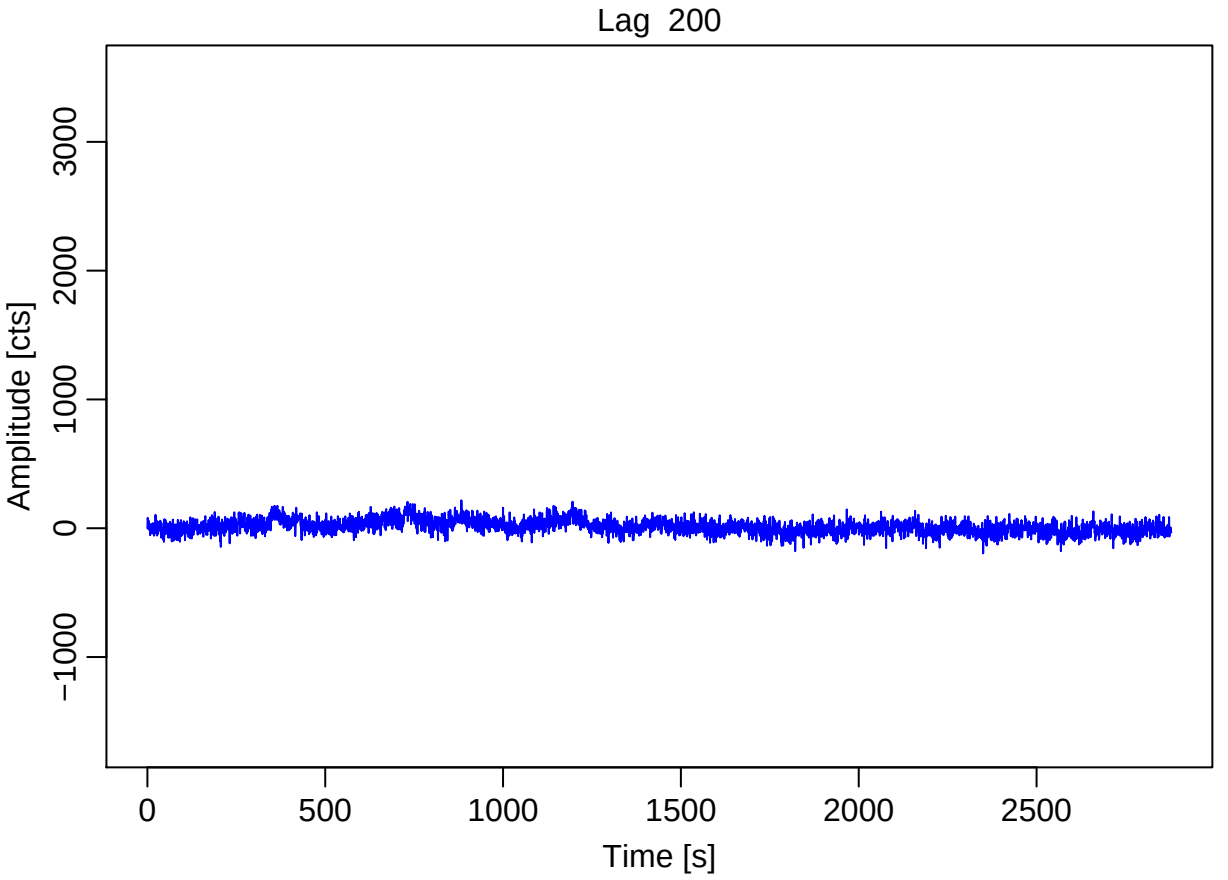
Lag 200
Amplitude [cts]
3000
2000
1000
0
−1000
0
500
1000
1500
2000
2500
Time [s]

Figure 13

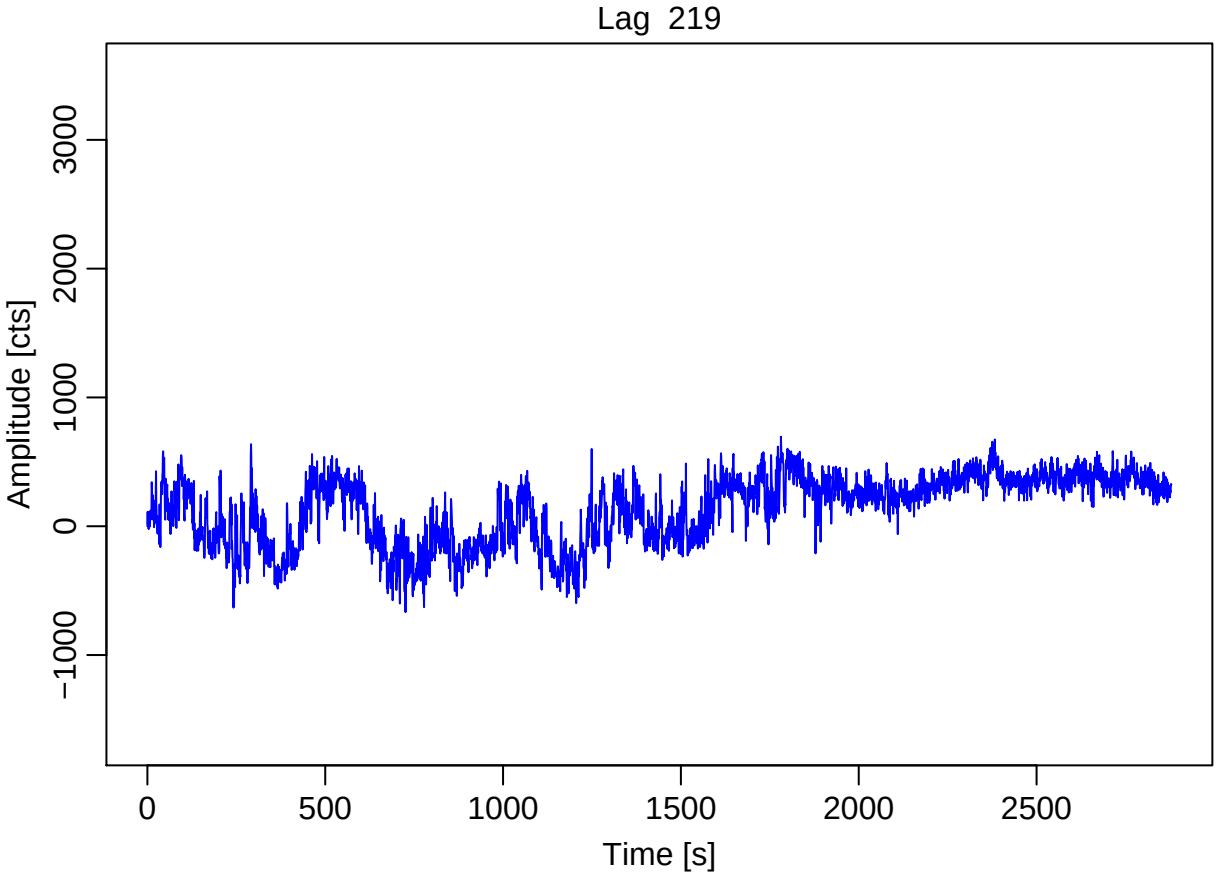
Lag 219
Amplitude [cts]
3000
2000
1000
0
−1000
0
500
1000
1500
2000
2500
Time [s]

Figure 14

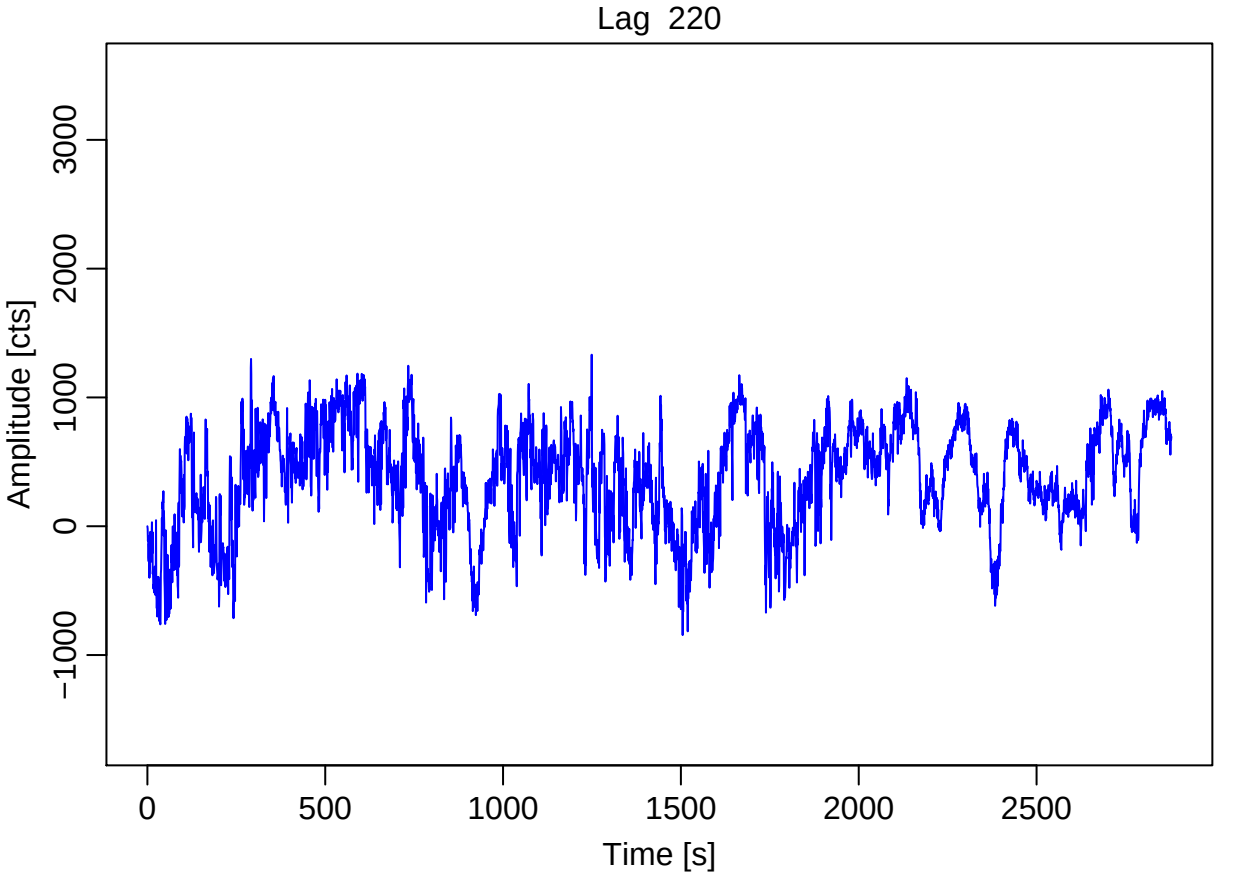
Lag 220
Amplitude [cts]
3000
2000
1000
0
−1000
0
500
1000
1500
2000
2500
Time [s]

Figure 15

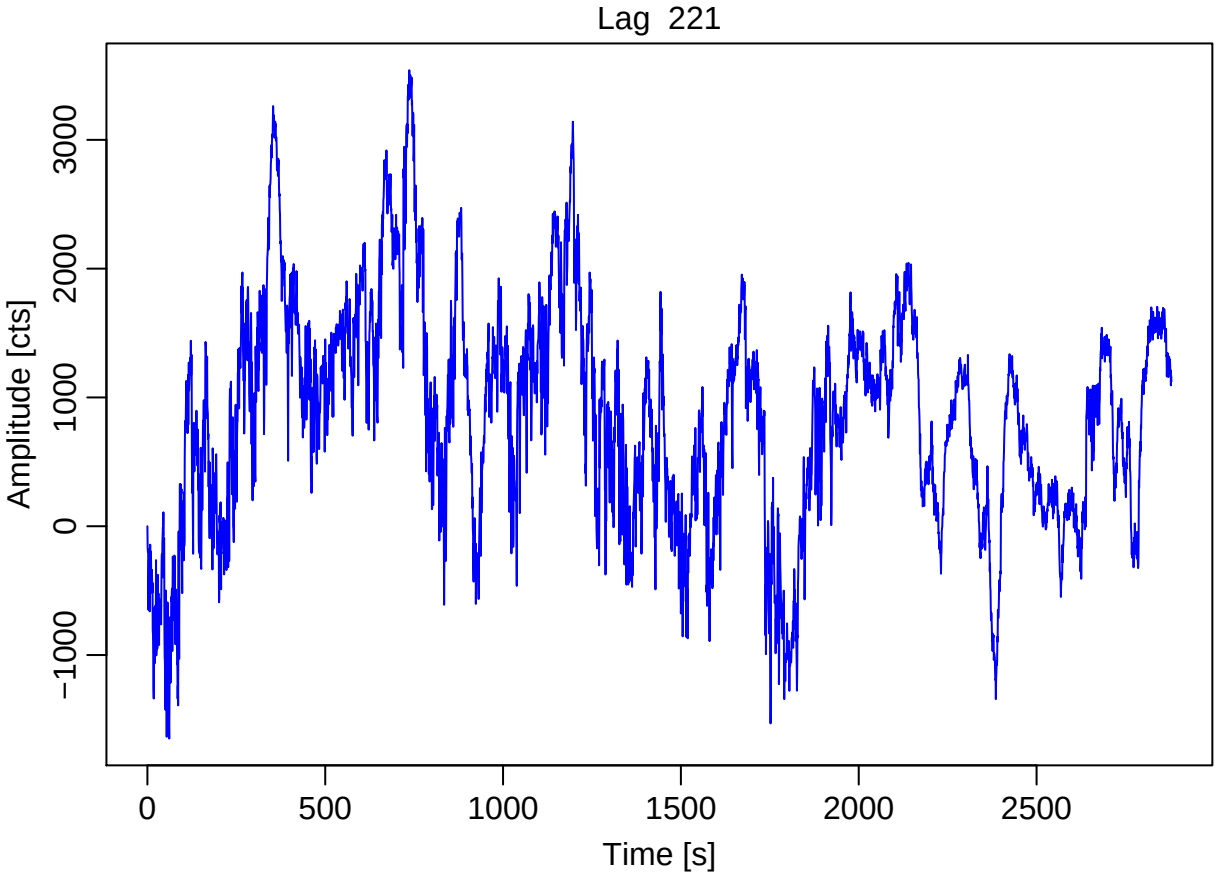
Lag 221
Amplitude [cts]
3000
2000
1000
0
−1000
0
500
1000
1500
2000
2500
Time [s]

Figure 16

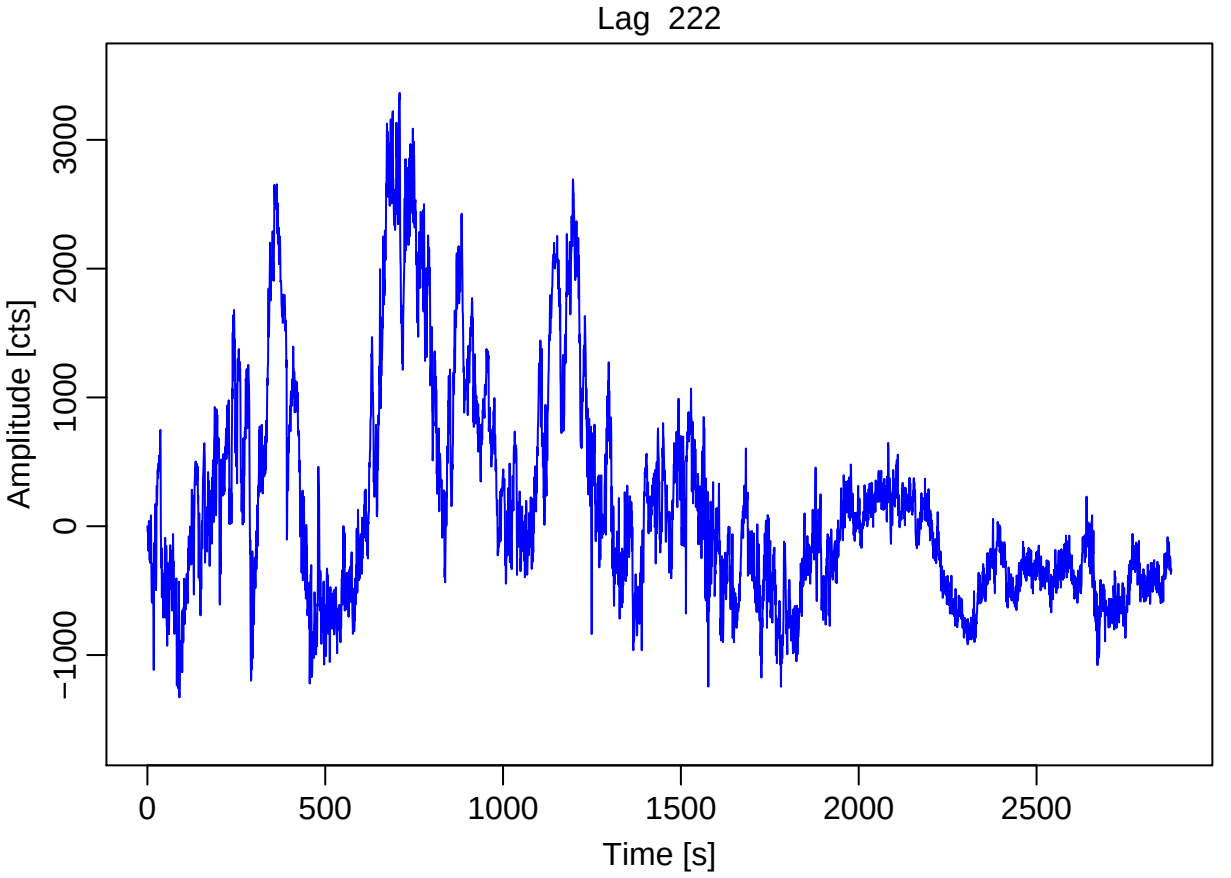
Lag 222
Amplitude [cts]
3000
2000
1000
0
−1000
0
500
1000
1500
2000
2500
Time [s]

Figure 17

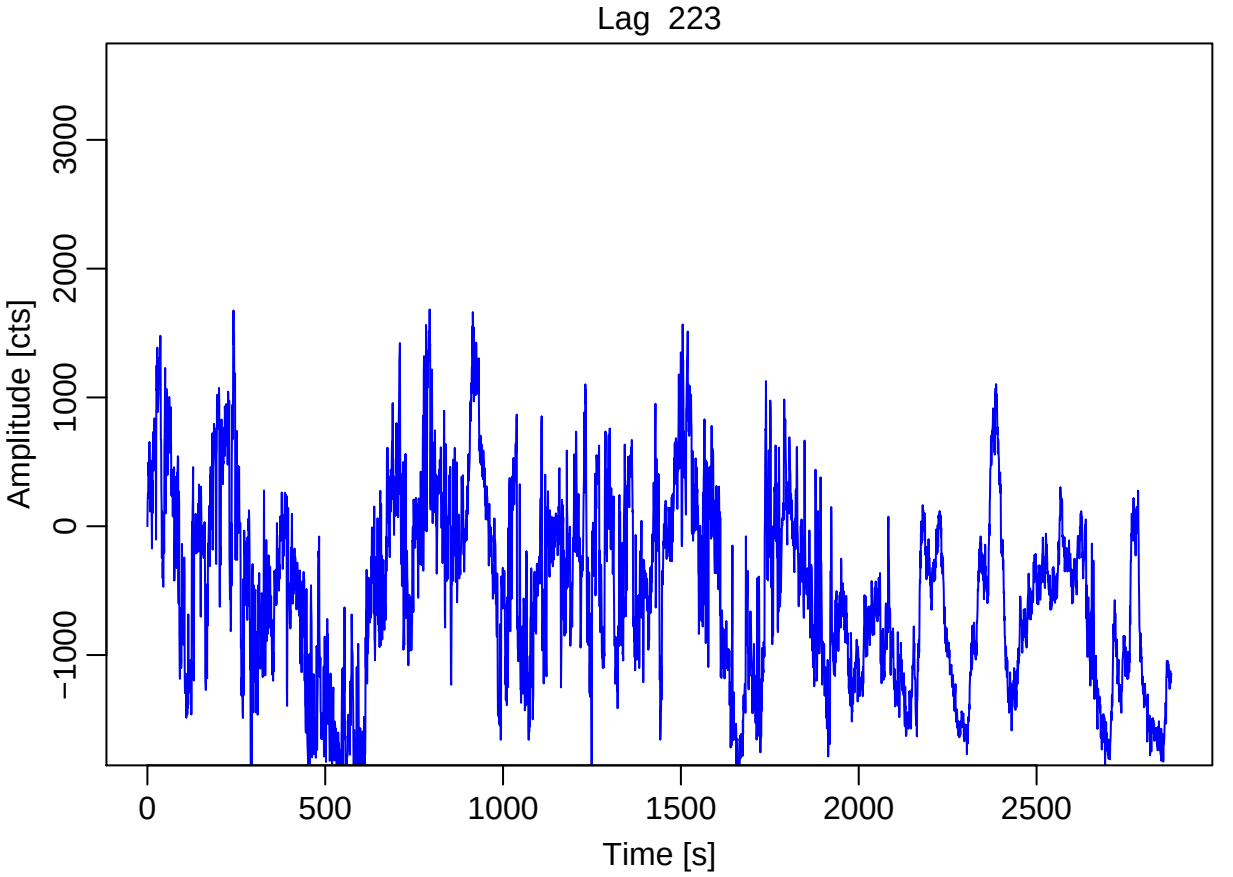
Lag 223
Amplitude [cts]
3000
2000
1000
0
−1000
0
500
1000
1500
2000
2500
Time [s]

Figure 18

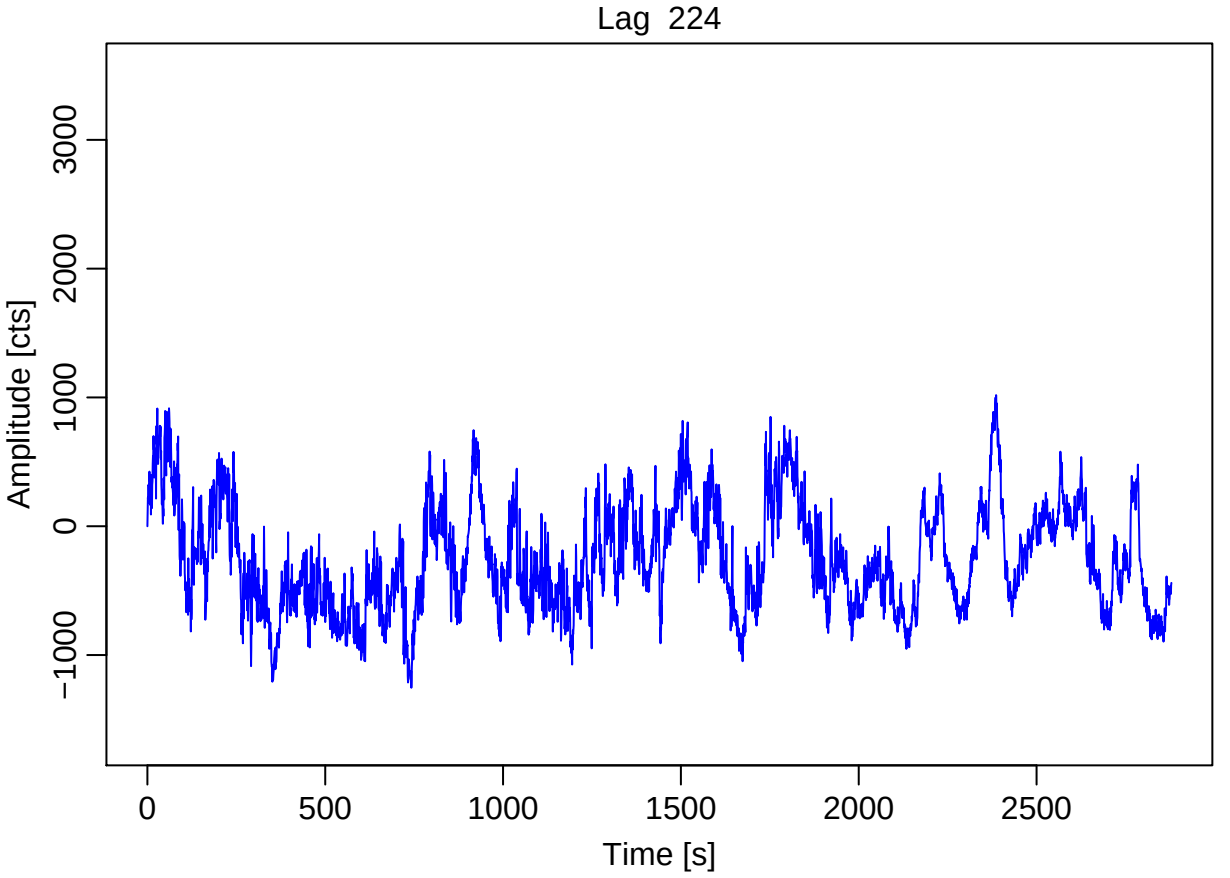
Lag 224
Amplitude [cts]
3000
2000
1000
0
−1000
0
500
1000
1500
2000
2500
Time [s]

Figure 19

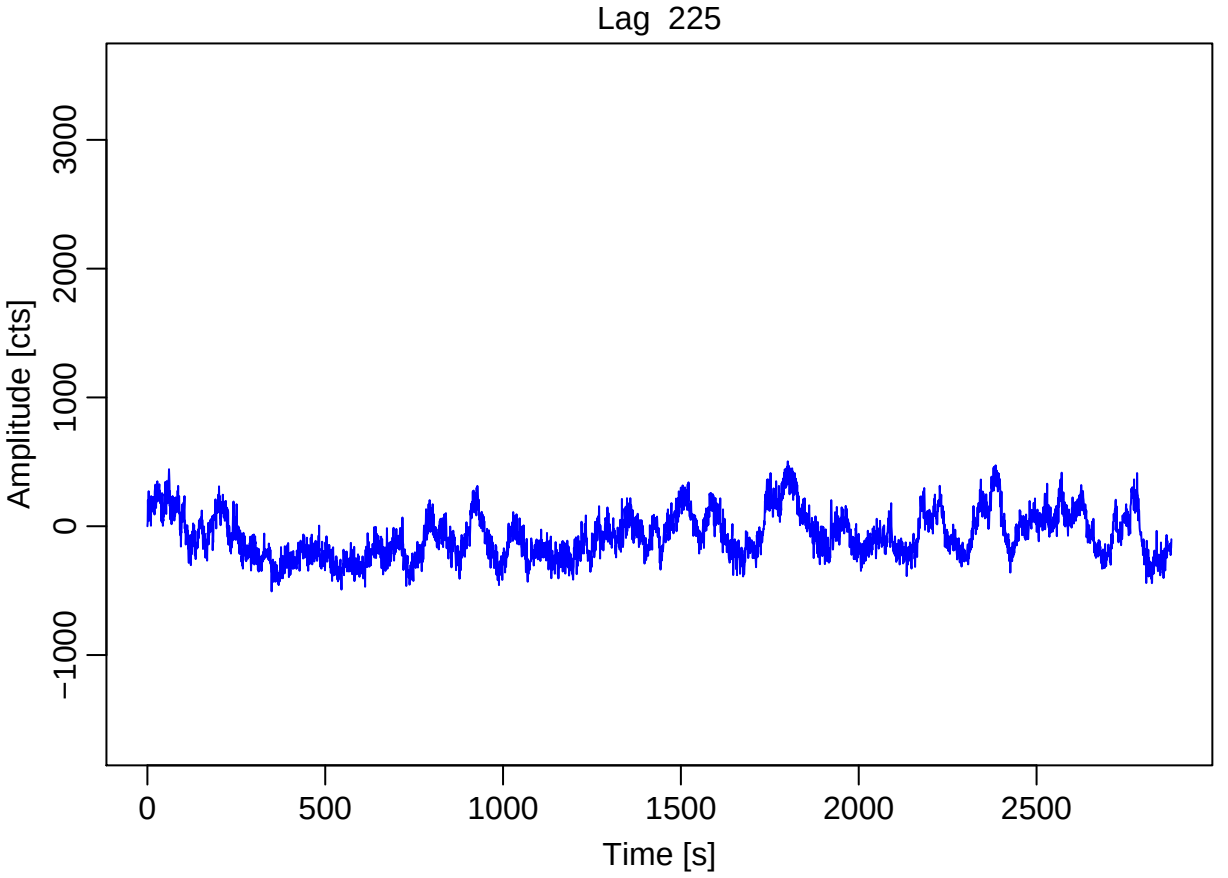
Lag 225
Amplitude [cts]
3000
2000
1000
0
−1000
0
500
1000
1500
2000
2500
Time [s]

Figure 20

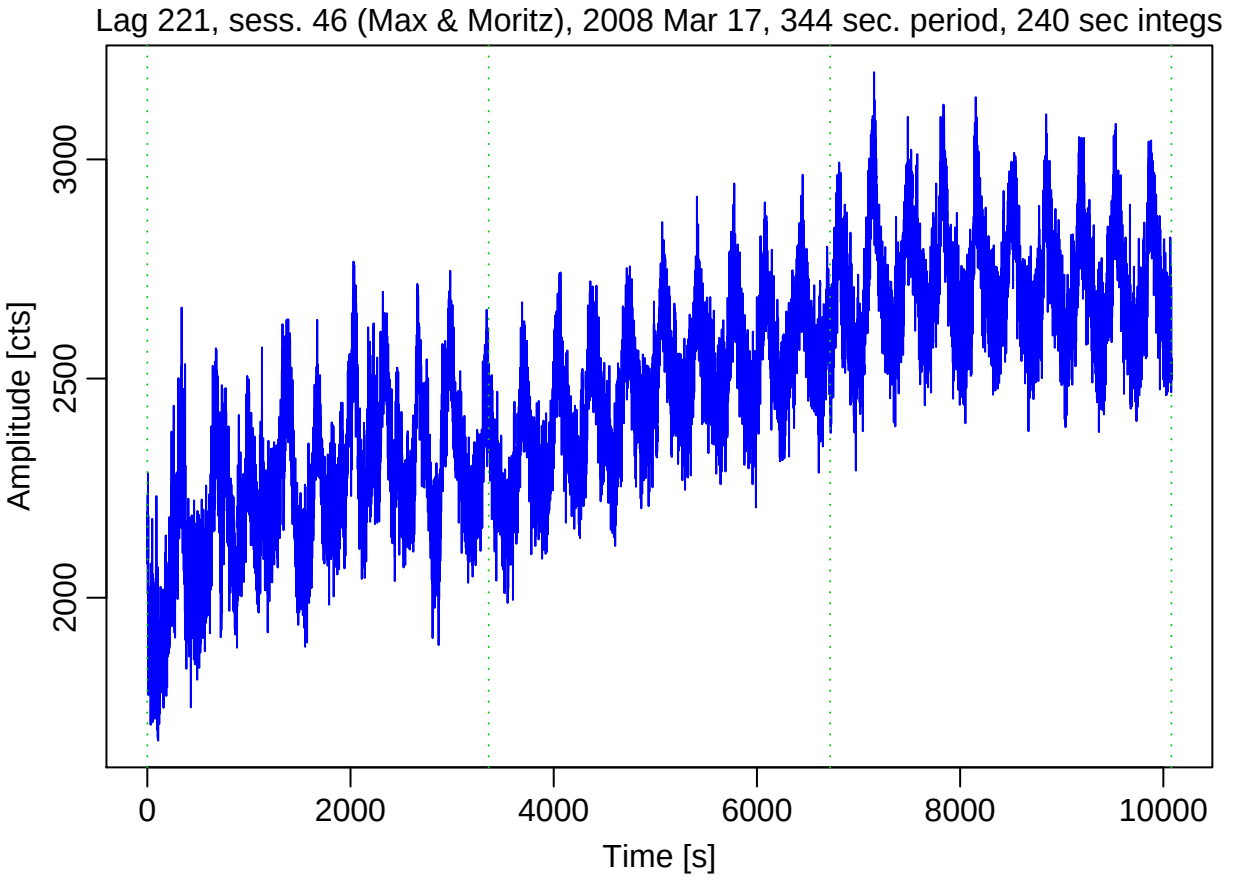
Lag 221, sess. 46 (Max & Moritz), 2008 Mar 17, 344 sec. period, 240 sec integs
Amplitude [cts]
2000
2500
3000
0
2000
4000
6000
8000
10000
Time [s]

Figure 21

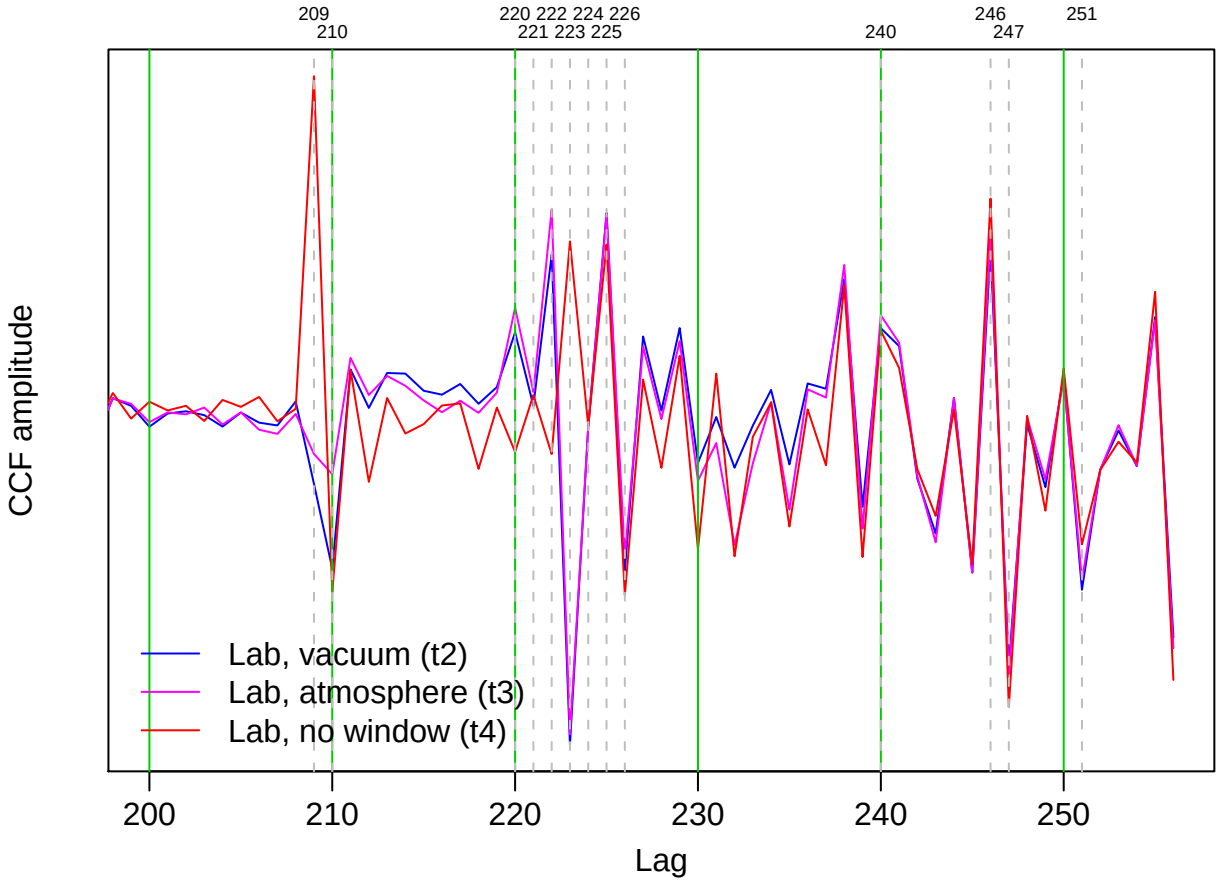
209
210
220 222 224 226
221 223 225
240
246
247
251
CCF amplitude
Lab, vacuum (t2)
Lab, atmosphere (t3)
Lab, no window (t4)
200
210
220
230
240
250
Lag

Figure 22

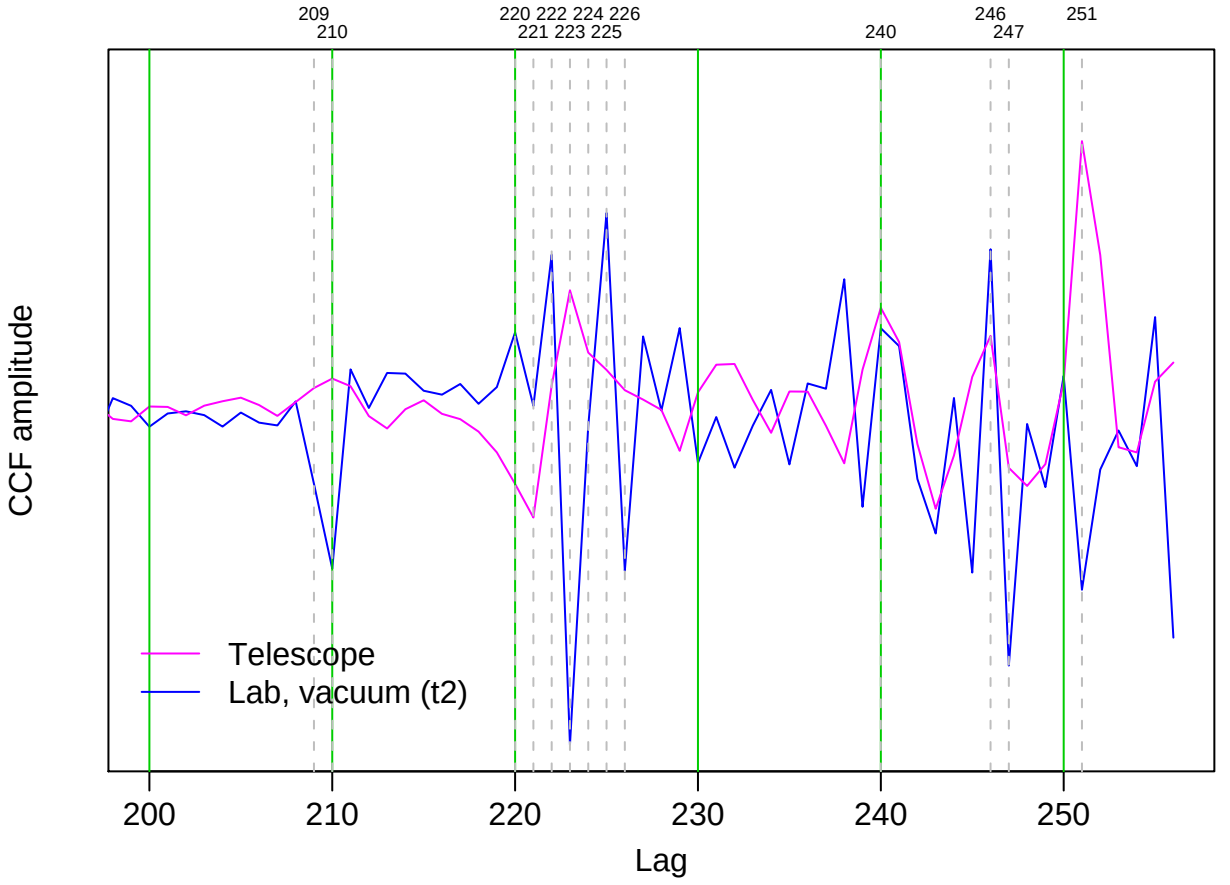
209
210
220 222 224 226
221 223 225
240
246
247
251
CCF amplitude
Telescope
Lab, vacuum (t2)
200
210
220
230
240
250
Lag

Figure 23

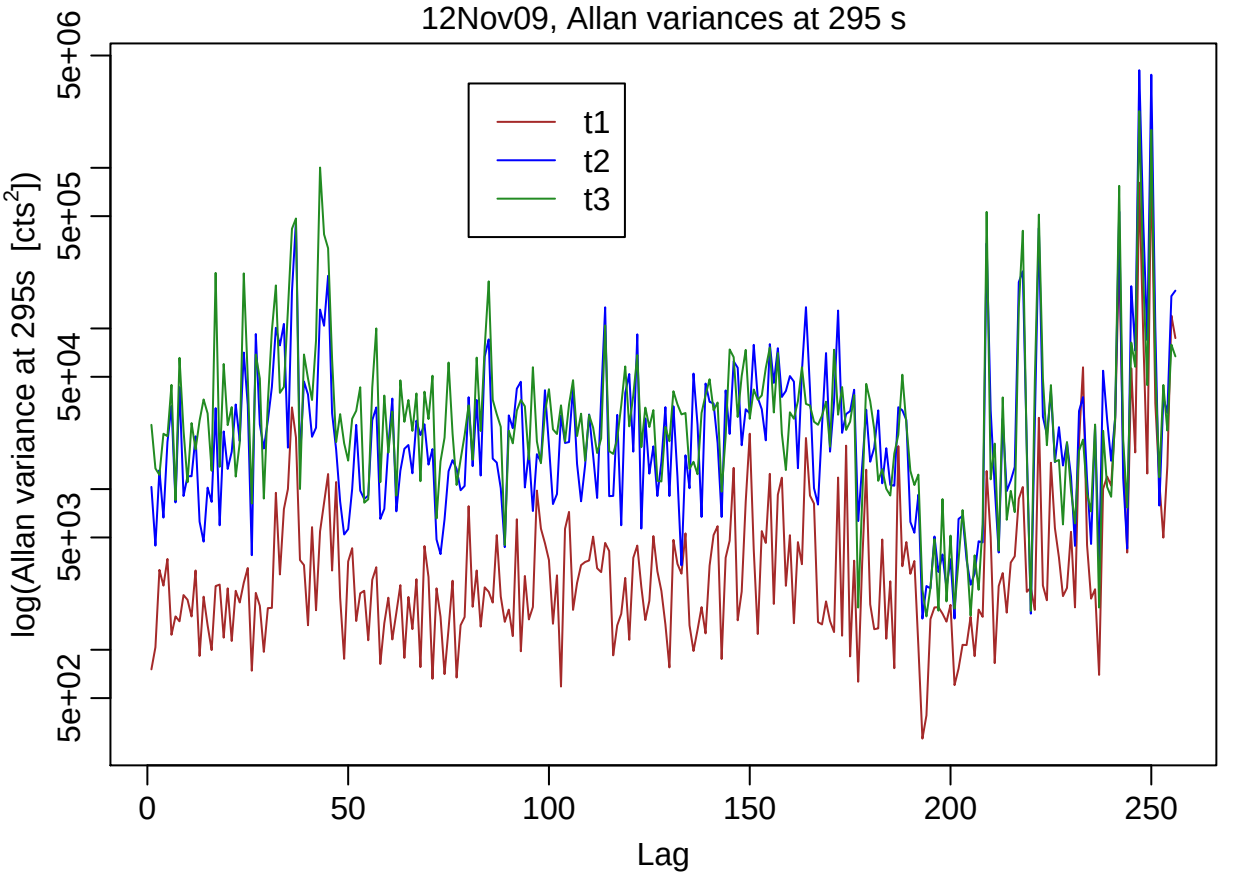
12Nov09, Allan variances at 295 s
log(Allan variance at 295s [cts^2])
5e+02
5e+03
5e+04
5e+05
5e+06
t1
t2
t3
0
50
100
150
200
250
Lag

Figure 24

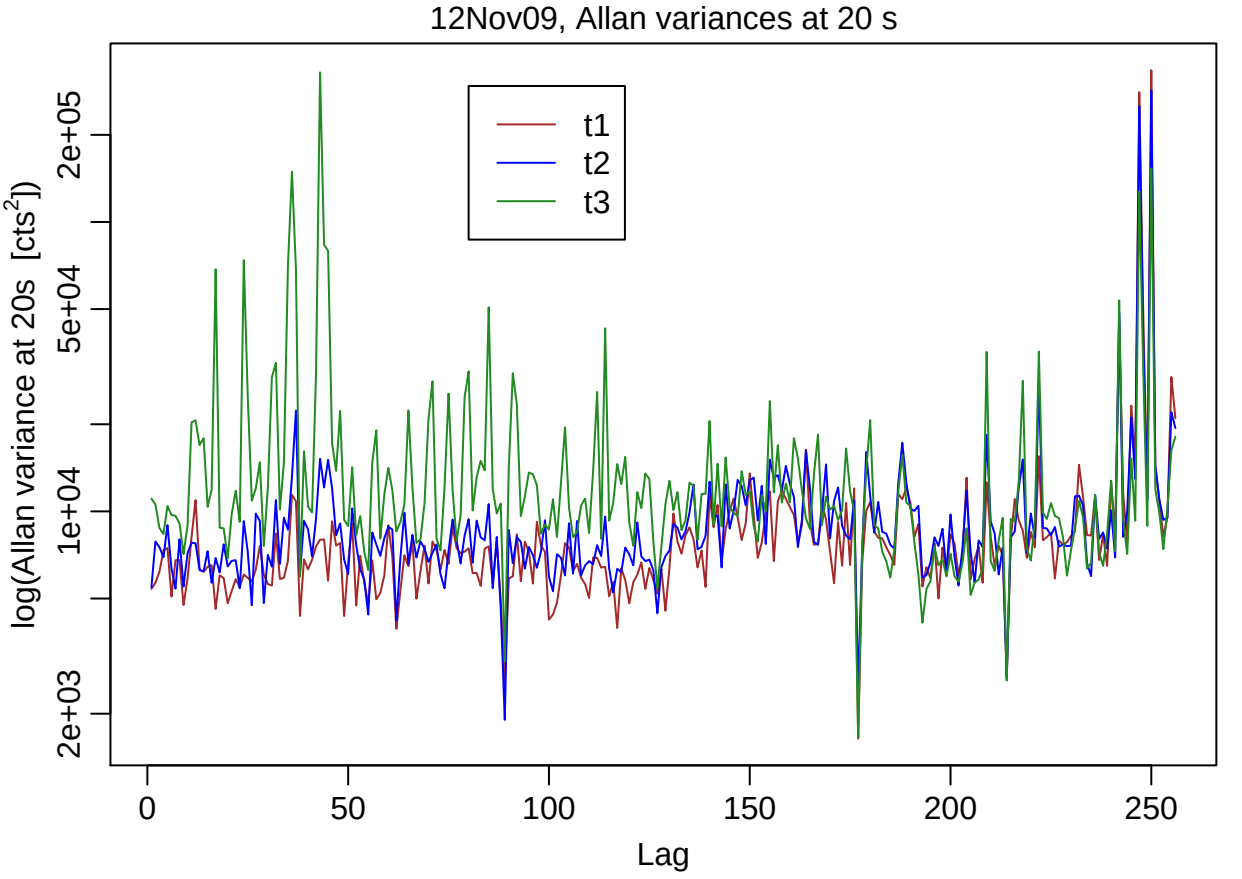
12Nov09, Allan variances at 20 s
t1
t2
t3
log(Allan variance at 20s [cts^2])
2e+03
1e+04
5e+04
2e+05
0
50
100
150
200
250
Lag

Figure 25

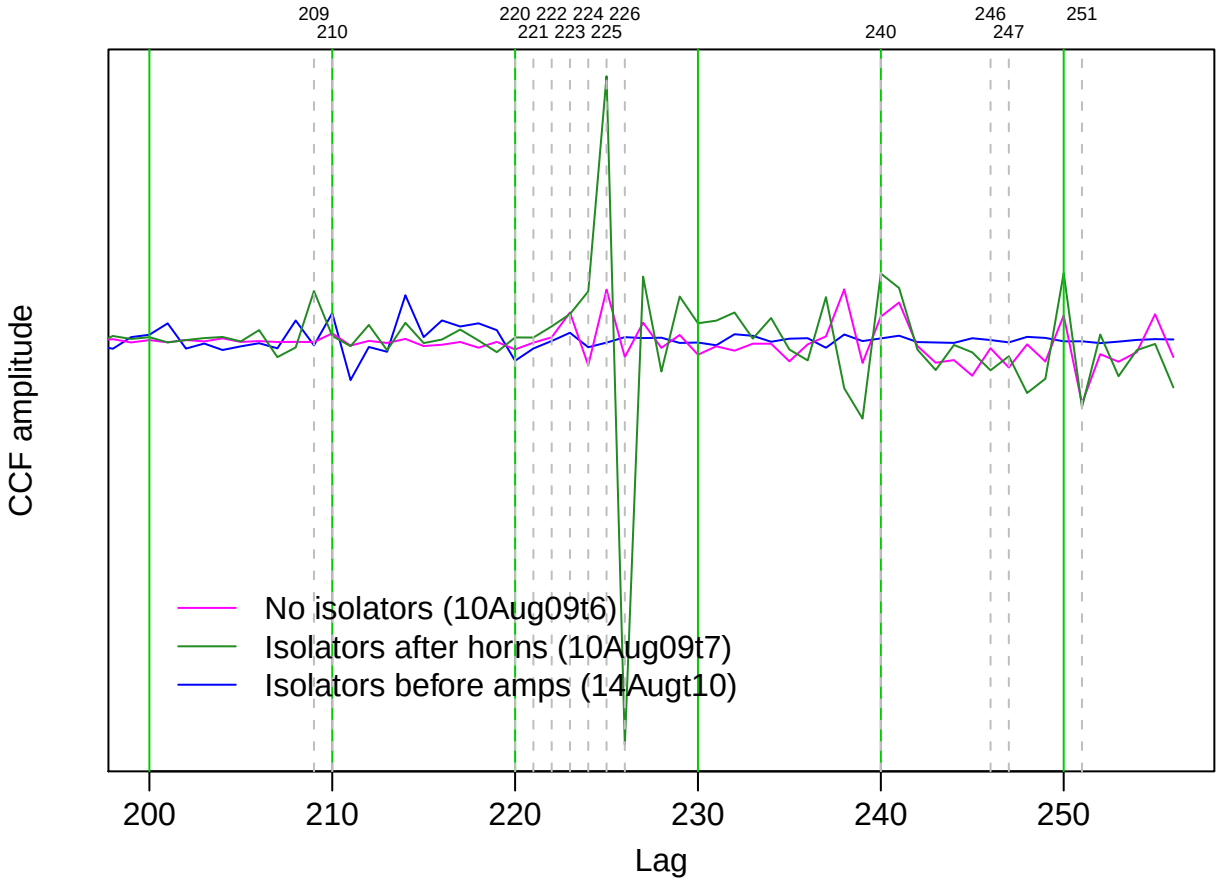
209
210
220 222 224 226
221 223 225
240
246
247
251
CCF amplitude
No isolators (10Aug09t6)
Isolators after horns (10Aug09t7)
Isolators before amps (14Augt10)
200
210
220
230
240
250
Lag

Figure 26